Journal of Medicinal Chemistry

Article

pubs.acs.org/jmc

# Structure-Based Design, Synthesis, and Evaluation of Peptide-Mimetic SARS 3CL Protease Inhibitors

Kenichi Akaji,*[,‡,†] Hiroyuki Konno,[§] Hironori Mitsui,[‡] Kenta Teruya,[‡] Yasuhiro Shimamoto,[‡] Yasunao Hattori,[‡] Takeshi Ozaki,[∥] Masami Kusunoki,[⊥] and Akira Sanjoh[#]

[†]Department of Medicinal Chemistry, Kyoto Pharmaceutical University, Yamashina-ku, Kyoto 607-8412, Japan

[‡]Department of Chemistry, Graduate School of Medical Science, Kyoto Prefectural University of Medicine, Kita-ku, Kyoto 603-8334, Japan

[§]Yamagata University, Yonezawa, Yamagata 992-8510, Japan

[∥]Institute for Protein Research, Osaka University, Suita, Osaka 565-0871, Japan

[⊥]University of Yamanashi, Kofu, Yamanashi 400-8511, Japan

[#]R&D Center, Protein Wave Co., Nara 631-0006, Japan

Supporting Information

**ABSTRACT:** The design and evaluation of low molecular weight peptide-based severe acute respiratory syndrome (SARS) chymotrypsin-like protease (3CL) protease inhibitors are described. A substrate-based peptide aldehyde was selected as a starting compound, and optimum side-chain structures were determined, based on a comparison of inhibitory activities with Michael type inhibitors. For the efficient screening of peptide aldehydes containing a specific C-terminal residue, a new approach employing thioacetal to aldehyde conversion mediated by *N*-bromosuccinimide was devised. Structural optimization was carried out based on X-ray crystallographic analyses of the R188I SARS 3CL protease in a complex with each inhibitor to provide a tetrapeptide aldehyde with an $IC_{50}$ value of 98 nM. The resulting compound carried no substrate sequence, except for a $P_3$ site directed toward the outside of the protease. X-ray crystallography provided insights into the protein−ligand interactions.

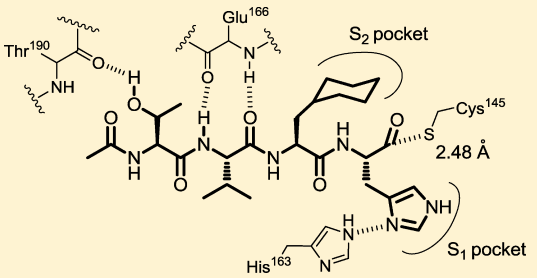


## INTRODUCTION

Severe acute respiratory syndrome (SARS), a life-threatening form of pneumonia, is caused by a new coronavirus (SARS CoV).[1−3] Although the primary SARS epidemic that affected about 8500 patients and left 800 dead was eventually brought under control, no effective therapy exists for this viral infection. In addition, the recent identification of a SARS CoV-like virus in Chinese bats raises the possibility of a re-emergence of SARS or related diseases.[4,5] Thus, developing anti-SARS agents against future outbreaks remains a formidable challenge.

SARS is a positive-sense, single-stranded RNA virus featuring the largest viral RNA genome known to date.[6,7] The genomic RNA produces two large proteins with overlapping sequences, polyproteins 1a (~450 kDa) and 1ab (~750 kDa), which are autocatalytically cleaved by two or three viral proteases to yield functional polypeptides.[8] The key enzyme in this processing is a 33 kDa protease, which is called the chymotrypsin-like protease (3CL).[9,10] The SARS 3CL protease is a cysteine protease with a chymotrypsin fold and cleaves precursor proteins at as many as 11 conserved sites involving a conserved Gln at the $P_1$ position and a small amino acid (Ser, Ala, or Gly) at the $P_1'$ position with varying efficiency.[11,12] The 3CL protease exists as a homodimer, and each 33 kDa protomer has its own active site containing a Cys-His catalytic dyad. Because of its functional importance in the viral life cycle, the 3CL protease is considered an attractive target for the structure-based design of drugs against SARS.[13−20] Several crystal forms of the SARS 3CL protease with or without inhibitors have also been used to evaluate various types of inhibitors for this protease.[10,21−25] Most inhibitors contain a functional group such as a chloromethyl ketone, a Michael acceptor, or an epoxide that can react irreversibly with the active-site cysteine residue. Few studies dealing with inhibitors containing an aldehyde group as a functional group have been reported.[26] In the course of our own studies on the SARS 3CL protease and its inhibitors,[27] we found that the mature SARS 3CL protease is sensitive to degradation at the 188Arg/189Gln site, which causes a loss of catalytic activity. The stability of the 3CL protease is dramatically increased by mutating the Arg at the 188 position to Ile. The enzymatic efficiency of the R188I mutant was increased by a factor of more than $1 \times 10^6$. The potency of the mutant protease makes it possible to quantitatively evaluate substrate-based peptide-aldehyde inhibitors using conventional high-performance liquid chromatography (HPLC). The evaluations revealed that a peptide aldehyde containing the substrate

Received: March 18, 2011
Published: October 20, 2011

P-site pentapeptide sequence, Ac-Ser-Ala-Val-Leu-NHCH-($CH_2CH_2CON(CH_3)_2$)-CHO **1**, inhibits the catalytic activity of the SARS 3CL protease with an $IC_{50}$ value of 37 $\mu$M (Figure 1).

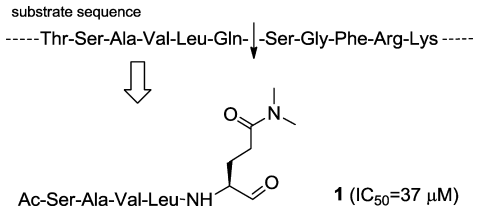


**Figure 1.** Structure of substrate-based peptide inhibitor.

To optimize the side-chain structures of the substrate-based inhibitor, we first confirmed the efficiency of the aldehyde group as an essential factor by comparing the inhibitory activity with that of a Michael type inhibitor. The findings indicate that the aldehyde type inhibitors are superior. The side-chain structures, especially at sites $P_1$, $P_2$, and $P_4$, were then optimized step by step based on X-ray crystallographic analyses of the inhibitor-protease complex. In parallel, for the solid-phase synthesis of a series of peptide-aldehydes, a new method was developed, involving an acetal linker and its efficient conversion to an aldehyde through the formation of a thioacetal.

## CHEMISTRY

Michael acceptor type inhibitors including homologated analogues were synthesized starting from commercially available Boc-L-Glu-OBn as shown in Scheme 1. The side-chain carboxyl group of Boc-L-Glu-OBn was converted to a dimethylamide by condensation with dimethylamine using benzotriazole-1-yl-oxy-tris-(dimethylamino)-phosphonium hexafluorophosphate (BOP)[28] as a coupling reagent. Consequent reduction of the benzylester with $LiAlH_4$ afforded the corresponding alchohol, Boc-L-Gln$(Me)_2$-ol **3**. For the synthesis of **5** with a typical $\alpha,\beta$-unsaturated carbonyl function, **3** was converted into an aldehyde, Boc-L-Gln$(Me)_2$-al, by Swern oxidation. Horner–Wadsworth–Emmons olefination using triethyl phosphonoacetate then gave the desired $N^{\alpha}$-protected amino acid ester **4**. The $N^{\alpha}$-protecting group of **4** was cleaved by TFA, and the product was coupled with the tetra-peptide Ac-Ser($^t$Bu)-Ala-Val-Leu-OH prepared by a conventional Fmoc-based solid-phase peptide synthesis. The side-chain *t*-butyl-protecting group was removed by TFA treatment, and the product **5** was purified by HPLC to give a single main peak. To prepare the elongated analogue **9**, Boc-L-Gln$(Me)_2$-al was homologated via the Wittig reaction using methoxymethyl triphenylphosphonium chloride followed by an acid treatment to yield the corresponding aldehyde **6**. The Horner–Wadsworth–Emmons olefination of **6** and coupling with the tetrapeptide as above afforded **9**. To prepare the analogue **10**, **6** was further homologated via the Wittig reaction and an acid treatment as above. The following Horner–Wadsworth–Emmons olefination and coupling with the tetrapeptide afforded **10**.

A conventional Weinreb amide resin[29] was employed to prepare the peptide aldehydes **11–16** containing different amino acid residues at the $P_1$ site. The corresponding amino acid residues were introduced by a conventional Fmoc-based solid-phase synthesis (Scheme 2). After construction of the peptide chain, each resin was reduced with $LiAlH_4$ according to a published procedure.[29] The desired products could be purified by HPLC, but the overall yields were fairly low (0.5–4.4%).

To achieve further optimization of the substrate-based peptide aldehyde inhibitor, we developed a new scheme for the solid-phase synthesis of peptide aldehydes containing a specific C-terminal residue. In 2007, an oxazolidine linker[30] was reported to be useul for the solid-phase synthesis of long-chain peptide aldehydes, as compared to known procedures such as the use of a Thr-based oxazolidine linker, acetal resin, or semicarbazide resin.[31] During the deprotection of this

**Scheme 1. Synthesis of Michael Acceptor Type Inhibitors 5, 9, and 10**[a]

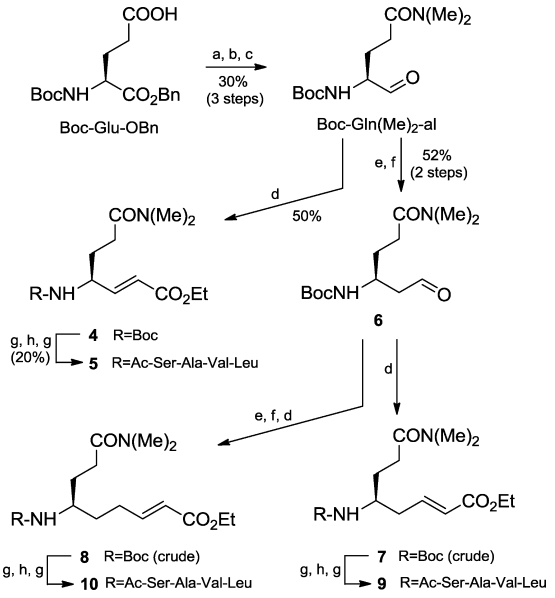


[a](a) BOP, $(Me)_2NH$, DIEA, 25 °C, 15 h. (b) $LiAlH_4$, 0 °C, 15 min: (c) DMSO, $(COCl)_2$, −40 °C, 2h. (d) $(EtO)_2POCH_2COOEt$, NaH, 25 °C, 90 min. (e) $MeOCH_2PPh_3Cl$, $Bu^tOK$, 25 °C, 1 h. (f) 1M HCl, 25 °C, 30 min. (g) TFA, $CH_2Cl_2$, 25 °C, 20 min. (h) Ac-Ser($Bu^t$)-Ala-Val-Leu-OH, WSC, HOOBt, DIEA, 25 °C, 12 h.

**Scheme 2. Solid-Phase Synthesis of Peptide Aldehyde Inhibitors 11–16**

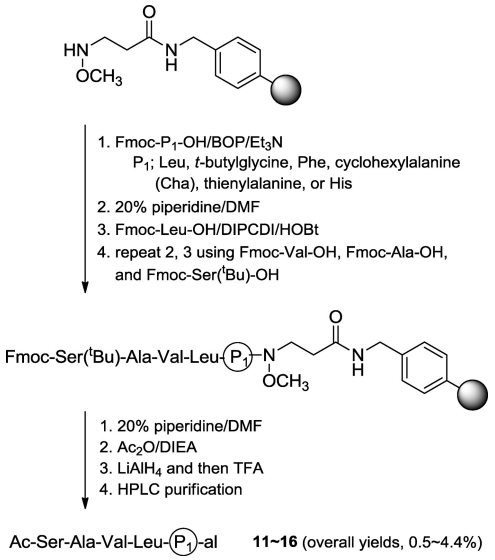



dx.doi.org/10.1021/jm200870n | J. Med. Chem. 2011, 54, 7962–7973

oxazolidine linker, however, a thioacetal compound was produced, more or less as a side product. In the present study, we found that the conversion of an acetal to an aldehyde is quite slow but that the thioacetal can be efficiently converted into the desired aldehyde by treatment with *N*-bromosuccinimide (NBS).

On the basis of this finding, the Fmoc-His(Trt)-acetal **19** containing a linker[32] was selected as a C-terminal residue (Scheme 3).

**Scheme 3. Solid-Phase Synthesis of Peptide Aldehyde Inhibitors 30−35**[a]

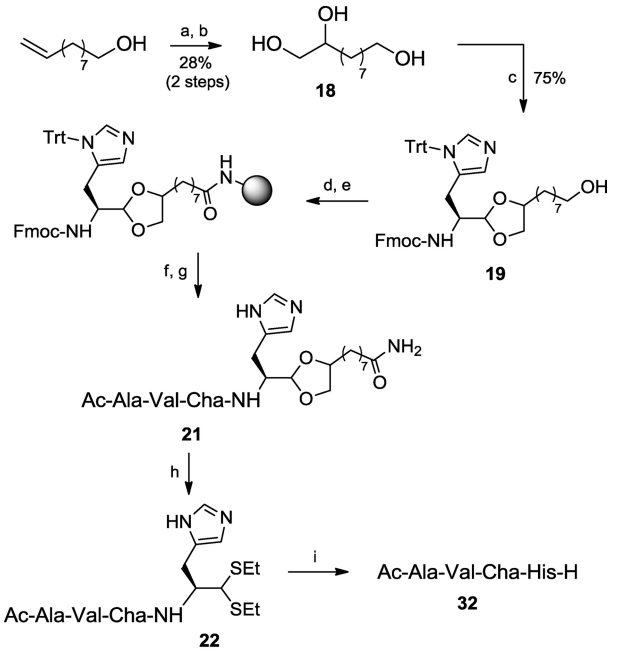


| compounds | peptide sequence |
|---|---|
| 22, 32; | Ac-Ala-Val-Cha- |
| 23, 33; | Ac-Asn-Val-Cha- |
| 24, 34; | Ac-Ser-Val-Cha- |
| 25, 35; | Ac-Thr-Val-Cha- |
| 26, 30; | Ac-Ser-Ala-Val-Phe- |
| 27, 31; | Ac-Ser-Ala-Val-Cha- |

[a](a) *m*CPBA, 25 °C, 30 min. (b) 1M NaOH, reflux, 2 h. (c) Fmoc-His(Trt)-al, $BF_3$-$Et_2O$, 25 °C, 30 min. (d) Jones reagent, 25 °C, 40 min. (e) Rink amide resin, DIPCDI, HOBt, DIEA, 25 °C, 10 h. (f) Fmoc-based peptide synthesis. (g) TFA-anisole, 25 °C, 4 h. (h) EtSH, $BF_3$-$Et_2O$, 25 °C, 2 h. (i) NBS, 25 °C, 1 min.

Epoxydation of the commercially available 9,10-decene-1-ol with *m*CPBA and hydrolysis gave a triol linker **18**. Fmoc-His(Trt)-al, prepared from the corresponding Weinreb amide, was then reacted with **18** in the presence of $BF_3$ etherate ($BF_3$-$Et_2O$) to yield the corresponding acetal **19**. The acetal alcohol was oxidized by treatment with the Jones reagent, and the resulting carboxylic acid, without any further purification, was anchored to a Rink amide resin[33] [4-(2,4-dimethoxyphenyl-Fmoc-aminomethyl)-phenoxy resin] using diisopropylcarbodiimide (DIPCDI)/1-hydroxybenzotriazole (HOBt) as the coupling reagents. The coupling of the corresponding amino acid residues was conducted by conventional Fmoc-based peptide synthesis using DIPCDI/HOBt coupling and Fmoc deprotection by treatment with piperidine. The product resin was treated with TFA to afford the desired peptide acetal amide **21**. The crude product was dissolved in AcOH and treated with ethanethiol in the presence of $BF_3$-$Et_2O$ as above. After that was quenched with $H_2O$, the desired thioacetal peptide **22** was easily purified by HPLC, although a prolonged reaction (more than 4 h) of the Ser-containing acetal-peptide may lower the yield due to acetylation of the Ser side-chain hydroxyl group. The thioacetal thus obtained was treated with NBS; the conversion required less than 1 min. The reaction mixture was immediately subjected to HPLC to give the desired peptide aldehyde **32** showing a single peak.

## RESULTS AND DISCUSSION

The inhibitory activities of Michael acceptor type derivatives were first evaluated based on $IC_{50}$ values (Table 1) according to a published procedure.[27] While the $IC_{50}$ of a previously reported peptide aldehyde **1** was reported to be 37 $\mu$M,[27] the value for **5**, containing the same peptide sequence as **1**, was 330 $\mu$M. The Michael type analogues **9** and **10** that had been elongated toward the prime site showed no inhibitory activities. These results suggest that the aldehyde type inhibitor containing the substrate sequence would be more active toward the R188I 3CL protease than the irreversible Michael type inhibitor. The results regarding analogues **9** and **10** also suggest that the recognition of the prime-site main-chain structure by the 3CL protease is strict and that no linker structure inserted between the $P_1$ site and the reactive functional group would be tolerated.

For optimization of the side-chain structures of **1**, optimization at the $P_1$ site was first necessary. Conversion of the side-chain structure at the $P_1$ site would be expected to have a dramatic effect on inhibitory activity, since the $P_1$ site is conserved in all cleavage sequences of the mature 3CL protease. Six different side-chain structures were examined (Table 2): aliphatic isobutyl and *tert*-butyl groups, aromatic and aliphatic ring structures, and heteroatom-containing ring structures. Each peptide aldehyde was prepared using a conventional Weinreb amide resin and purified by HPLC, but the overall yields were not impressive.

The inhibitory activities of the synthesized aldehydes were evaluated based on $IC_{50}$ values calculated from a decrease in the substrate by protease digestion in the presence of different inhibitor concentrations. Incubation of the protease with an inhibitor prior to the addition of the substrate gave an $IC_{50}$

**Table 1. Inhibitory Activities of Michael Type Inhibitors**

| compd | structure | $IC_{50}$ ($\mu$M) |
|---|---|---|
| **1** | Ac-Ser-Ala-Val-Leu-NHCH($CH_2CH_2CON(CH_3)_2$)-CHO | 37 |
| **5** | Ac-Ser-Ala-Val-Leu-NHCH($CH_2CH_2CON(CH_3)_2$)-CH=CHCOOEt | 330 |
| **9** | Ac-Ser-Ala-Val-Leu-NHCH($CH_2CH_2CON(CH_3)_2$)-$CH_2$−CH=CHCOOEt | Nl[a] |
| **10** | Ac-Ser-Ala-Val-Leu-NHCH($CH_2CH_2CON(CH_3)_2$)-$(CH_2)_2$−CH=CHCOOEt | Nl |

[a]Nl, no inhibition.


dx.doi.org/10.1021/jm200870n | *J. Med. Chem.* 2011, 54, 7962−7973

**Table 2. Inhibitory Activities of Pj Site-Substituted Peptide Aldehydes**

| compound | structure | $IC_{50}$ (μM) |
|---|---|---|
| 1 | 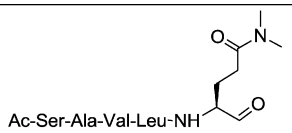 | 37 |
| 11 | 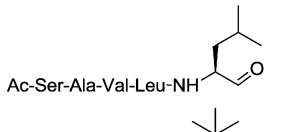 | ~3000 |
| 12 | 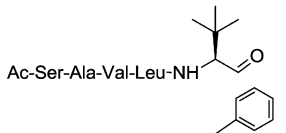 | ~3000 |
| 13 | 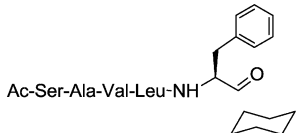 | ~2000 |
| 14 | 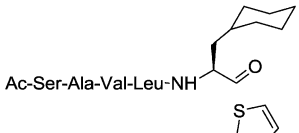 | 62 |
| 15 | 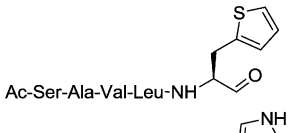 | 48 |
| 16 | 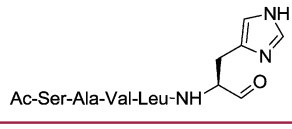 | 5.7 |

value that was not significantly different from that obtained when the inhibitor and substrate were mixed simultaneously. Typical sigmoidal curves and $IC_{50}$ values (4.0 μM by preincubation vs 5.7 μM by simultaneous mixing) obtained by these two procedures for **16** are shown in Figure S-1 in the Supporting Information. These results suggest that the inhibitory mode of the aldehyde inhibitor does not involve a suicide mechanism, since the presence of a large excess of inhibitor (μM scale inhibitor vs nM scale protease) had no effect on the cleavage of the substrate when it was added afterward. Thus, the $IC_{50}$ values summarized in Table 2 were obtained using a simple simultaneous mixing procedure. Replacement with an aliphatic group or an aromatic ring abolished the inhibitory activity (compounds **11**−**13**), but replacement with a cyclohexyl or a thiophen structure had little effect on the inhibitory activity (**14** and **15**). In contrast, replacement with an imidazole ring (**16**) increased the inhibitory activity by more than 6-fold as compared to **1**. From these results, the pentapeptide aldehyde **16** containing a His unit at the $P_1$ site was selected as a lead compound for further optimization.

To achieve further optimization using a structure-based design, crystallization and X-ray crystallographic analyses of the R188I mutant protease and its inhibitor complex were conducted. The structure of the mutant protease containing no inhibitor (PDB code: 3AW1) was first refined to a resolution of 2.00 Å (data collection and refinement statistics are summarized in Table 3).

As compared with the reported mature 3CL protease (PDB code: 2ZU4), X-ray crystallography revealed that the R188I mutation did not cause any major change in the overall tertiary organization of the SARS 3CL protease (Figure 2A). The electron density at the active site Cys145 and the dimer's interface, such as residues Ser139-Leu141,[34] was clearly detected, and the expected dimeric structure was folded similarly to the mature protease. The side chain of the mutated Ile was directed toward the outside of the protease, and the electron density at the mutated site was nearly the same as that of structures lacking the guanidine group of Arg in the mature protease (Figure 2B).

**Table 3. Data Collection and Refinement Statistics for the R188I SARS 3CL Protease and Its Inhibitor in Complexes with Compounds 16, 31, and 35**

| PDB ID | 3AW1 | 3AW0 | 3AVZ | 3ATW |
|---|---|---|---|---|
| | without inhibitor | complexed with **16** | complexed with **31** | complexed with **35** |
| space group | *P*1 | C121 | C121 | *P*1 |
| unit cell parameters | | | | |
| length *a* | 52.13 | 108.384 | 109.185 | 54.517 |
| length *b* | 67.454 | 81.606 | 80.533 | 58.546 |
| length *c* | 67.384 | 53.33 | 52.987 | 67.745 |
| angle *α* | 71.23 | 90 | 90 | 94.29 |
| angle *β* | 77.46 | 104.24 | 105.05 | 104.03 |
| angle *γ* | 81.74 | 90 | 90 | 106.64 |
| resolution | 30.0−2.00 | 50.0−2.30 | 50.0−2.50 | 46.4−2.30 |
| observations | 212842 | 145804 | 113847 | 61338 |
| unique observations | 51940 | 19005 | 14594 | 29416 |
| redundancy | 3.8 | 7.3 | 7.4 | 2 |
| completeness | 97.2 | 99.9 | 97.4 | 96.7 |
| mean $I/\sigma(I)$ | 24.2 | 21.8 | 16.7 | 11.8 |
| *R* merge | 0.038 | 0.082 | 0.122 | 0.079 |
| resolution range | 30.0−2.00 | 50.0−2.30 | 50.0−2.50 | 46.4−2.30 |
| $R_{cryst}$ | 0.22 | 0.23 | 0.22 | 0.23 |
| $R_{free}$ | 0.26 | 0.29 | 0.26 | 0.3 |
| rmsd from ideal | | | | |
| bond length (Å) | 0.023 | 0.022 | 0.018 | 0.01 |
| bond angle (deg) | 2.007 | 1.943 | 1.781 | 1.308 |


dx.doi.org/10.1021/jm200870n | J. Med. Chem. 2011, 54, 7962−7973

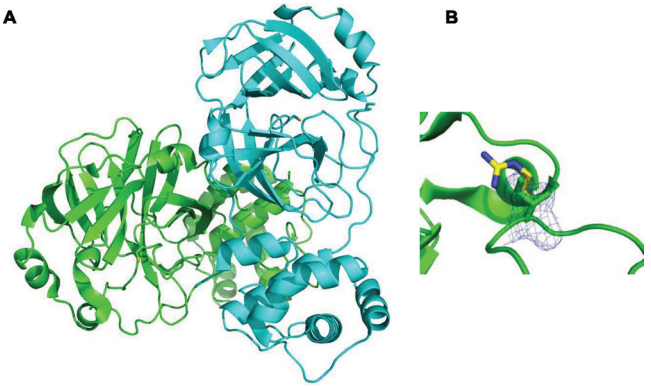


**Figure 2.** (A) Overall dimeric organization of the R188I mutant protease; side chain structures of the mutated Ile and active center Cys are shown as a stick model. (B) Structures near the mutated Ile residue superimposed on the mature 3CL protease (PDB code 2ZU4). The Match Maker Program in the UCSF Chimera package was utilized for superimposing 2ZU4 on 3AW1.

The structure of the mutant protease, in a complex with the lead compound **16**, was refined to a resolution of 2.30 Å (Table 3). The X-ray crystallography revealed that the overall structure was folded similar to the R188I mutant protease solved above. Each monomer of the dimer contains the inhibitor **16** at its active center (PDB code: 3AW0). The binding did not cause changes in the overall organization of the dimer, and **16** was located in the active site cleft. The carbonyl carbon of the aldehyde in **16** was detected at a sufficiently close distance (2.30 Å) from the thiol of the active center Cys-145, and its electron density could be fitted to an $sp^2$ carbonyl carbon (Figure 3A). The side-chain imidazole nitrogen of the $P_1$ site His formed a hydrogen bond with His-163 of the mutant protease, which placed the other side of the $P_1$ site imidazole into a $S_1$ pocket formed from the side chains of Phe-140, Leu-141, and Glu-166 of the protease (Figure 3-B). The isobutyl group of the $P_2$ site Leu was located at the $S_2$ pocket made by Met-45, Met-165, and His-41, but some space still remained from Met-45 and -165 (Figure 3C). The amide-bound nitrogen and carbonyl oxygen atoms of the $P_3$-Val of **16** formed hydrogen bonds with the protease main chain at Glu-166, and the amide-bound nitrogen of the $P_4$-Ala of **16** also formed a hydrogen bond with the protease main chain at Thr-190. Although those hydrogen bonds hold the main chain of the inhibitor into the active-site cleft of the protease, side chains of the $P_3$-Val and the $P_5$-Ser were directed to the outside of the protease, and no interaction with the protease was detected at these sites (Figure 3).

On the basis of these structural analyses, small molecular inhibitors containing an aldehyde functional group were designed as follows. First, the side chain of the $P_2$ site was replaced with a bulky group to permit the side chain to fit into the $S_2$ pocket more tightly than **16**. Next, the outwardly directed $P_5$ site was removed to lower the molecular weight of the inhibitors, since no interactions at the corresponding side chains with the protease were detected. Third, to more closely attach the $P_5$ site-deleted inhibitor to the active-site cleft, a heteroatom was introduced into the side chain of the $P_4$ site to create the possibility of additional hydrogen bonds with the protease. Thus, six additional inhibitors (**30**–**35** in Table 4) were designed and synthesized using the newly developed acetal-thioacetal conversion method (Scheme 3).

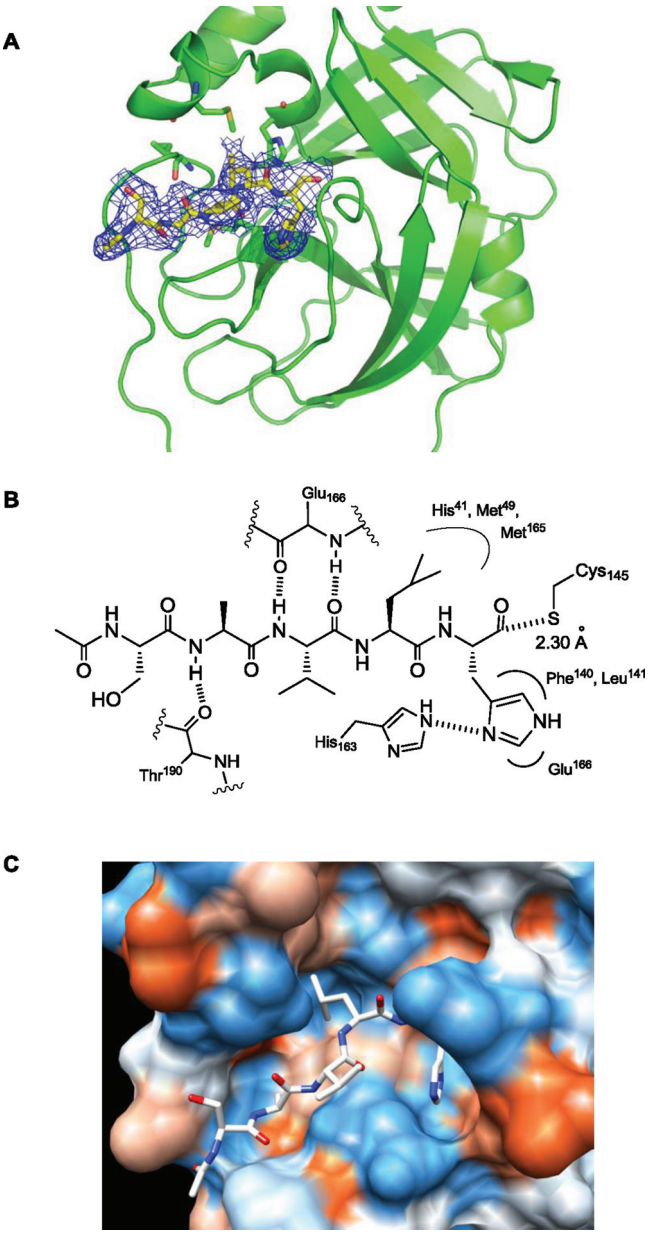


**Figure 3.** (A) X-ray structure of the inhibitor **16** bound to the R188I SARS 3CL protease (PDB code 3AW0); oxygen (red), nitrogen (blue), and sulfur (yellow); the main chain of **16** is also shown in yellow. (B) Mode of the interaction. (C) Molecular graphics image produced using the UCSF Chimera package from the Resource for Biocomputing Visualization, and Informatics at the University of California, San Francisco (supported by NIH P41 RR-01081).

The inhibitory activities of the newly synthesized inhibitors were evaluated using $IC_{50}$ values obtained by the simultaneous mixing procedure, as detailed above (Table 4). The peptide aldehydes containing a more bulky phenyl or cyclohexyl group at the $P_2$ site showed dramatically increased inhibitory activity (compounds **30** and **31**) as expected. Substitution with a cyclohexyl group was more effective than substitution with a planar aromatic group, and the inhibitory activity of **31** was increased by more than 80 times as compared with **16** (a reduction in the $IC_{50}$ value from 5.7 $\mu$M to 65 nM).[35] Reducing the molecular weight of **31** caused by the simple deletion of the $P_5$ site lowered the inhibitory activity to 1/6, but the resulting compound **32** was still 20 times more potent than the lead


dx.doi.org/10.1021/jm200870n | J. Med. Chem. 2011, 54, 7962–7973

**Table 4. Inhibitory Activities of $P_2$ and $P_4$ Site-Substituted Peptide Aldehydes**

| compound | structure | $IC_{50}$ (nM) |
|---|---|---|
| 16 | 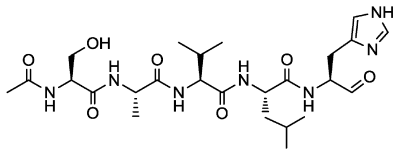 | 5700 |
| 30 | 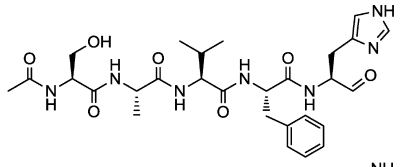 | 390 |
| 31 | 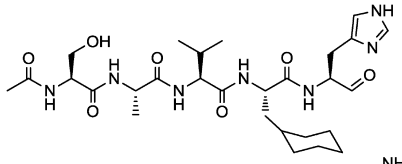 | 65 |
| 32 | 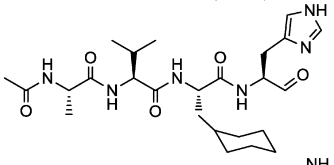 | 270 |
| 33 | 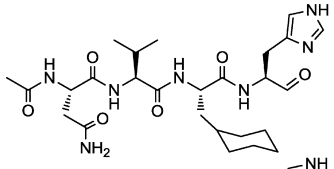 | 10000 |
| 34 | 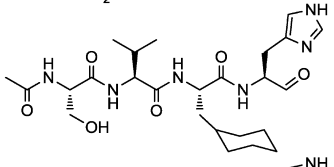 | 340 |
| 35 | 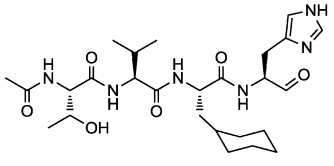 | 98 |

compound **16** (5.7 $\mu$M vs 270 nM in $IC_{50}$). The inhibitory activity of **32** was nearly the same as that of the $P_2$-replaced pentapeptide inhibitor **30**. Replacement of the $P_4$ site of **32** with an oxygen-containing side chain to create an additional hydrogen bond was then examined. Replacement of the $P_4$ site Ala with Ser to introduce an alcohol group at the side chain produced no significant increase in the inhibitory effect of **32**, although introducing an amide group by replacement with Asn resulted in a remarkable lowering in the inhibitory activity of **32**. In contrast, the introduction of a more hindered secondary alcohol at the $P_4$ site, replacement with Thr instead of Ser, gave a tetrapeptide aldehyde **35** having nearly the same inhibitory activity ($IC_{50}$ = 98 nM) as the pentapeptide aldehyde **31** ($IC_{50}$ = 65 nM). Thus, the molecular weight of the inhibitor was reduced to 534 for **35** from 591 for **31**, while the inhibitory activity remained the same.

The mode of binding of the small molecular inhibitor **35** was confirmed by X-ray crystallography as above (PDB code: 3ATW). The structure of the mutant protease in a complex with **35** was refined to a resolution of 2.30 Å (Table 3). The overall fitting of the inhibitor **35** was similar to that of **16**, but

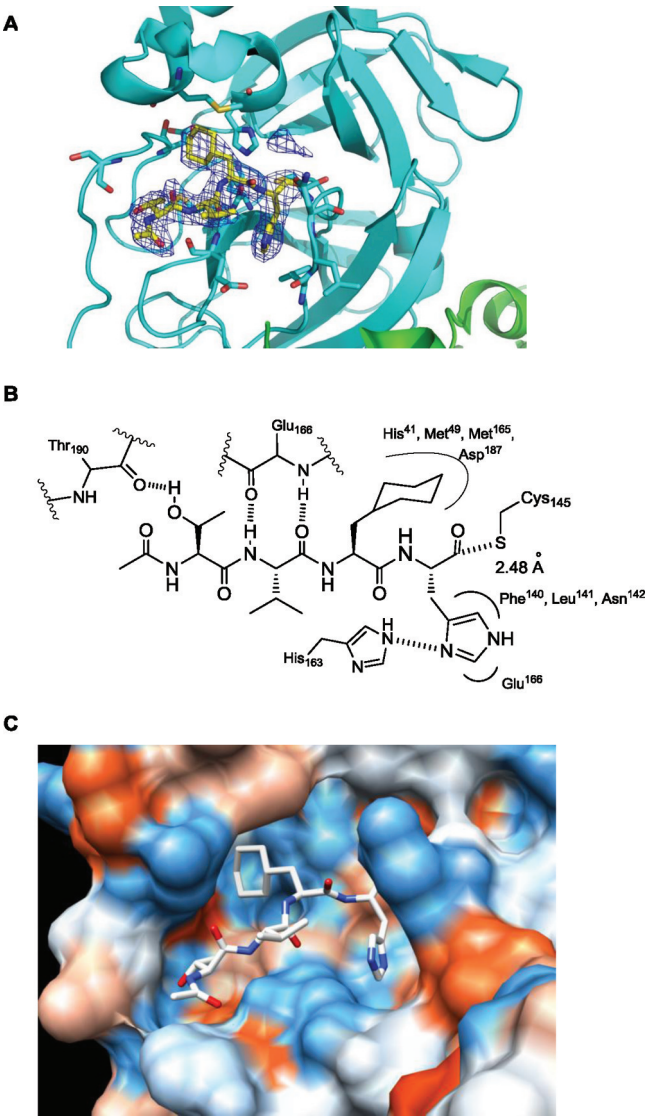


**Figure 4.** (A) X-ray structure of the inhibitor **35** bound to the R188I SARS 3CL protease (PDB code 3ATW); oxygen (red), nitrogen (blue), and sulfur (yellow); main chain of **35** is also shown in yellow. (B) Mode of the interaction. (C) Molecular graphics image produced using the UCSF Chimera package from the Resource for Biocomputing Visualization, and Informatics at the University of California, San Francisco (supported by NIH P41 RR-01081).

tight interactions were observed, especially at the $P_2$ and $P_4$ sites (Figure 4A). The carbonyl carbon of the aldehyde group in **35** was detected at a distance of 2.48 Å from the active center thiol of Cys-145, and its electron density could be fitted to an $sp^2$ carbonyl carbon as in **16**. The nitrogen atom of the $P_1$ site imidazole of **35** formed a hydrogen bond with the imidazole nitrogen of His-163, and the inhibitor imidazole was slightly twisted as compared to **16** (Figure 3), resulting in close fitting at the other side of the $S_1$ pocket formed from the Phe-140, Leu-141, and Glu-166 side chains of the protease. The cyclohexyl group at the $P_2$ site of **35** was inserted into a large $S_2$ pocket created by His-41, Met-49, Met-165, and Asp-187. Most of the S2 pocket was occupied by a cyclohexyl group, as shown in Figure 4C. The carbonyl oxygen and amide nitrogen atom of the $P_3$ site Val of **35** formed hydrogen bonds with Glu-166 of the protease, as observed in **16**. The side-chain oxygen of Thr at the $P_4$ site formed an additional hydrogen bond with


dx.doi.org/10.1021/jm200870n | J. Med. Chem. 2011, 54, 7962–7973

Thr-190 of the protease, which was not observed in the interaction with **16**. Those interactions, especially at the $P_1$, $P_2$, and $P_4$ sites, function to hold the main chain of the truncated inhibitor tightly into the active site cleft, which resulted in the compact fitting of the tetra-peptide inhibitor **35** to the mutant protease.

In these X-ray structural analyses of inhibitors bound to the mutant protease, the electron density of the aldehyde group in the inhibitors could be fitted to an expected $sp^2$ carbon. In the inhibitory assays, no significant difference was observed between the $IC_{50}$ value obtained after preincubation of the inhibitor with the protease and that obtained by simultaneous mixing (Figure S-1 in the Supporting Information). These results strongly suggest that the aldehyde inhibitor functions as a competitive inhibitor and that no stable covalent bonds are formed with the protease. To estimate the inhibitory mechanism, an inhibitory kinetics experiment with **35** was performed by collecting a Lineweaver–Burk plot.

The rate of cleavage for different amounts of substrate [S] by the R188I mutant protease in the absence or presence of **35** (25, 50, or 100 nM) was monitored during the initial 10–15 min reaction period using HPLC. The enzymatic reaction rate ($v$, $\mu$M/min) was obtained by monitoring the decrease in the area corresponding to the substrate, and the resulting $1/v$ was plotted against 1/S. The plots resulted in four straight lines with the same $y$-axis intercept reflecting competitive inhibition toward the protease [Figure 5, each plot obtained at each inhibitor concentration (0, 25, 50, or 100 nM) was shown in Figures S-2–S-5 in the Supporting Information].

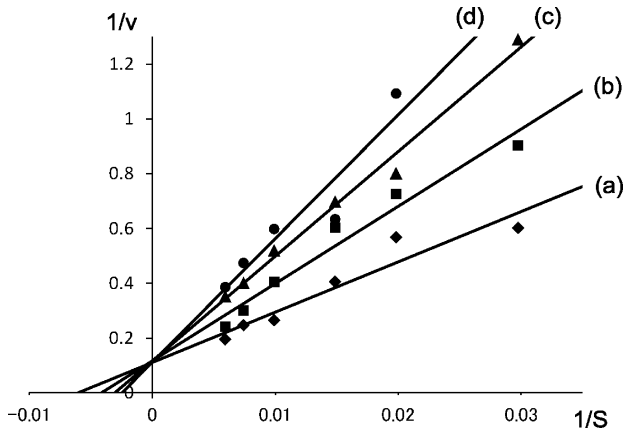


**Figure 5.** (a) Incubated without inhibitor; (b) incubated with 25 nM of **35**; (c) incubated with 50 nM of **35**; (d) incubated with 100 nM of **35**.

## CONCLUSION

SARS 3CL protease inhibitors containing an aldehyde at the C terminus were found to be more effective than an irreversible inhibitor containing a Michael acceptor at the same site. The initial lead sequence, Ac-Ser-Ala-Val-Leu-His-H **16** ($IC_{50}$ = 5.7 $\mu$M), was selected by the screening of $P_1$ site residues of a previously reported peptide aldehyde inhibitor, **1**. Systematic modification guided by the X-ray crystal structure of the lead compound-bound R188I SARS 3CL protease resulted in the production of a small molecular weight inhibitor **35** with an $IC_{50}$ value of 98 nM. All of the side-chain structures of **35** differed from the substrate sequence except at the $P_3$ site, where the side-chain was directed outward and no evidence was found for interactions with the protease. Kinetic inhibition data for **35** obtained from Lineweaver–Burk plots suggested that inhibitors containing an aldehyde at the C terminus can be expected to function as a competitive inhibitor. The interactions of the inhibitor **35** at the $P_1$ and $P_2$ sites with the protease seemed remarkably effective, and further modification of **35** into a nonpeptide inhibitor focusing on $P_1$ and $P_2$ site interactions is currently underway in our laboratory.

## EXPERIMENTAL SECTION

**General.** All solvents were of reagent grade. THF was distilled from sodium and benzophenone ketyl. $CH_2Cl_2$ was distilled from $CaH_2$. All commercial reagents were of the highest purity available. Analytical TLC was performed on silica gel (60 F-254, 0.25 mm plates). Column chromatography was carried out on Wakogel 60 (particle size, 63–200 $\mu$m) or Wakogel FC-40 (particle size, 20–40 $\mu$m). NMR spectra were recorded on a Bruker AM-300 or Bruker-DMX 500. Chemical shifts are expressed in ppm relative to TMS (0 ppm) or $CHCl_3$ (7.28 ppm). High-resolution mass spectra (HRMS) were obtained on a JMS-HX-110A (FAB), Bruker Autoflex-II (MALDI-TOF), or Bruker Daltonics HCTplus (ESI). The purity of the test compounds was determined by HRMS and HPLC. All test compounds showed ≥95% purity.

**Boc-NHCH[$CH_2CH_2CON(CH_3)_2$]-OBn (2).** To a solution of Boc-Glu-OBn (1.0 g, 3.0 mmol) and BOP (2.0 g, 4.5 mmol) in $CH_2Cl_2$ (10 mL) were added dimethylamine hydrochloride (0.49 g, 6.0 mmol) and DIEA (1.6 mL, 9.0 mmol), and the mixture was stirred for 15 h at room temperature. The reaction was quenched with saturated aqueous $NH_4Cl$, and the entire solution was extracted with AcOEt. The organic layer was washed with brine, dried over $Na_2SO_4$, filtered, and concentrated. The residue was purified by silica gel column chromatography using $CHCl_3$:MeOH (50:1, v/v) to give 1.1 g (98%) of **2** as a colorless solid, mp 97–99 °C. $[\alpha]_D^{24}$ −10.4° ($c$ 1.00, $CHCl_3$). $^1$H NMR ($CDCl_3$, 300 MHz): $\delta$ 1.43 (s, 9H) 1.98–2.07 (m, 1H), 2.14–2.27 (m, 1H), 2.30–2.40 (m, 2H), 2.89 (s, 3H), 2.92 (s, 3H), 4.30 (dd, $J$ = 12.0 Hz, 7.5 Hz, 1H), 5.13 (d, $J$ = 12.3 Hz, 1H), 5.21 (d, $J$ = 12.3 Hz, 1H), 5.43 (d, $J$ = 7.2 Hz, 1H), 7.30–7.37 (m, 5H). $^{13}$C NMR ($CDCl_3$, 75 MHz): $\delta$ 27.5, 28.3, 29.3, 35.5, 37.0, 53.5, 67.0, 79.8, 128.3, 128.3, 128.5, 135.5, 155.6, 171.8, 172.3. MS (ESI) $m/z$: 365.2 $[M + H]^+$.

**(4*S*)-4-[*N*-(*tert*-Butoxycarbonyl)amino]-5-hydroxypentanoic Acid (*N*,*N*-Dimethyl)amide, Boc-Gln(Me)$_2$-ol (3).** To a suspension of $LiAlH_4$ (0.11 g, 2.8 mmol) in THF (2.0 mL) was added benzyl ester **2** (0.50 g, 1.4 mmol) in THF (2.0 mL) at 0 °C, and the mixture was stirred for an additional 15 min at the same temperature. The reaction was quenched with water, and the resulting solution was extracted with AcOEt. The organic layer was washed with brine, dried over $Na_2SO_4$, filtered, and concentrated. The residue was purified by silica gel column chromatography using $CHCl_3$:MeOH (20:1, v/v) to give 0.26 g (72%) of **3** as colorless oil. $[\alpha]_D^{25}$ −13.4° ($c$ 2.05, $CHCl_3$). $^1$H NMR ($CDCl_3$, 300 MHz): $\delta$ 1.44 (s, 9H), 1.82–1.97 (m, 2H), 2.37–2.43 (m, 2H), 2.96 (s, 3H), 3.02 (s, 3H), 3.57 (brs, 2H), 3.74 (brs, 1H), 5.24 (brs, 1H). $^{13}$C NMR ($CDCl_3$, 125 MHz): $\delta$ 25.7, 28.3, 29.6, 35.6, 37.2, 52.7, 64.4, 79.2, 156.2, 173.1. MS (ESI) $m/z$: 261.3 $[M + H]^+$.

**Ethyl {(2*E*,4*S*)-4-[*N*-(*tert*-Butoxycarbonyl)amino]-7-one-7-dimethylamino}-2-heptenoate (Boc-NHCH[$CH_2CH_2CON(CH_3)_2$]-CH=CHCOO$C_2H_5$) (4).** To a stirred solution of oxaly chloride (4 mL, 47 mmol) in $CH_2Cl_2$ (100 mL) were added DMSO (6.6 mL, 93 mmol) and Boc-Gln(Me)$_2$-ol **3** (5.5 g, 21 mmol) in $CH_2Cl_2$ (40 mL), and the mixture was stirred at −40 °C for 2 h. After $Et_3N$ (30 mL, 0.21 mol) was added, the mixture was washed with $H_2O$ and brine. The organic phase was dried with $MgSO_4$, and the solvent was evaporated. The residue was partially purified by silica gel column chromatography using $CHCl_3$:MeOH (95:5, v/v) to afford 2.3 g (41%) of Boc-Gln(Me)$_2$-al. $^1$H NMR (300 MHz, $CDCl_3$): $\delta$ 1.20 (s, 9H), 1.56 (m, 1H), 1.72 (m, 1H), 2.19 (m, 2H), 2.71 (s, 3H), 2.79 (s, 3H), 4.29 (brt, $J$ = 8.7 Hz, 1H), 5.04 (brd, $J$ = 8.7 Hz, 1H), 9.34 (brs). The product was used without further purification. To a stirred solution of NaH (0.37 g, 15 mmol) in THF (15 mL) was added

triethyl phosphonoacetate (3.1 mL, 15 mmol), and the mixture was stirred at 4 °C for 30 min. Boc-Gln(Me)$_2$-al (2.0 g, 7.6 mmol) was added, and the mixture was stirred at 25 °C for 90 min. Ether (100 mL) was added, and the organic layer was washed with $H_2O$ and then brine, dried, and evaporated. The residue was purified by silica gel column chromatography using $CHCl_3$ to yield 1.2 g (50%) of **4**. $^1$H NMR (300 MHz, $CDCl_3$): $\delta$ 1.28 (t, $J$ = 7.2 Hz, 3H), 1.45 (s, 9H), 1.89−2.06 (m, 2H), 2.41 (t, $J$ = 7.1 Hz, 2H), 2.97 (s, 3H), 3.01 (s, 3H), 4.21 (q, $J$ = 7.2 Hz, 2H), 4.31 (brs, 1H), 5.08 (brs, 1H), 5.94 (d, $J$ = 15.9 Hz, 1H), 6.87 (dd, $J$ = 5.3 Hz, 15.9 Hz, 1H).

**Ac-Ser-Ala-Val-Leu-NHCH[$CH_2CH_2CON(CH_3)_2$]CH=CHCOO$C_2H_5$ (5).** To a stirred solution of Boc-NHCH-[$CH_2CH_2CON(CH_3)_2$]CH=CHCOO$C_2H_5$ **4** (17 mg, 52 $\mu$mol) in $CH_2Cl_2$ (0.4 mL) was added TFA (0.12 mL), and the mixture was stirred at 25 °C for 20 min. The solvent was removed by evaporation. The residue, after it was washed with hexane, was dissolved in DMF (1 mL). To the solution were added Ac-Ser($^t$Bu)-Ala-Val-Leu-OH (prepared by conventional Fmoc-based SPPS; 25 mg, 52 $\mu$mol), WSC (water-soluble carbodiimide) (16 mg, 104 $\mu$mol), 3-hydroxy-1,2,3-benzotriazine-4-one (HOOBt) (10 mg, 68 $\mu$mol), and DIEA (14 $\mu$L, 78 $\mu$mol), and the mixture was stirred at 25 °C for 12 h. The solvent was removed by evaporation, and the residue was dissolved in AcOEt (10 mL). The organic phase was washed with 5% citric acid, 5% $NaHCO_3$, and brine and dried. The solvent was removed, and the residue was dissolved in TFA (30 $\mu$L). The solution was allowed to stir at 25 °C for 1 h and was then evaporated. After it was washed with ether, the residue was dissolved in MeOH and purified by semipreparative HPLC using a Cosmosil 5C18 (10 mm × 250 mm) column to yield 7 mg (20%) of **5** showing a single peak on analytical HPLC: $R_t$ 12.99 min ($CH_3CN$ gradient; 20−45% in 30 min). MALDI TOF-MS. Calcd, 663.370 for $C_{30}H_{52}N_6O_9Na$; found, 663.653 for $[M + Na]^+$.

**Ac-Ser-Ala-Val-Leu-NHCH[$CH_2CH_2CON(CH_3)_2$]$CH_2$CH=CHCOO$C_2H_5$ (9).** To a stirred solution of methoxymethyltriphenylphosphonium chloride (11.5 g, 34 mmol) in THF (150 mL) was added $^t$BuOK (3.7 g, 34 mmol). The mixture was stirred at 25 °C for 30 min, and Boc-Gln(Me)$_2$-al (1.75 g, 6.7 mmol) in THF (30 mL) was added. The resulting solution was further stirred at 25 °C for 1 h and quenched with saturated aqueous $NH_4Cl$. The crude product was partially purified by silica gel column chromatography using $CHCl_3$, and the product, containing a small amount of methoxymethyltriphenylphosphonium chloride, was dissolved in THF (31 mL). To the solution was added 1 N HCl (6.2 mL), and the mixture was stirred at 25 °C for 30 min and quenched with a saturated aqueous solution of $NH_4Cl$. The crude product was extracted with $CH_2Cl_2$, and the organic phase was washed with $H_2O$ and then brine, dried over $MgSO_4$, and evaporated. The residue was purified by silica gel column chromatography using $CHCl_3$ to afford 0.95 g (52%) of Boc-NHCH[$CH_2CH_2CON(CH_3)_2$]$CH_2$CH=O **6**. $^1$H NMR (300 MHz, $CDCl_3$): $\delta$ 1.42 (s, 9H), 1.86−1.93 (m, 1H), 2.40 (brt, $J$ = 7.4 Hz, 2H), 2.65 (brd, $J$ = 6.0 Hz, 2H), 2.95 (s, 3H), 3.00 (s, 3H), 3.97−4.09 (m, 1H), 5.08 (brd, $J$ = 7.5 Hz, 1H), 9.76 (brs). The aldehyde was reacted with triethyl phosphonoacetate, and the resulting crude product **7** was treated with TFA followed by hexane washing as above to afford $NH_2CH[CH_2CH_2CON(CH_3)_2]CH_2CH{=}CHCOOC_2H_5$. $^1$H NMR (300 MHz, $CDCl_3$): $\delta$ 1.27 (t, $J$ = 7.2 Hz, 3H), 1.89−1.96 (m, 2H), 2.52−2.72 (m, 4H), 2.96 (s, 3H), 3.07 (s, 3H), 3.44 (tt, $J$ = 6.3 Hz, 6.3 Hz, 1H), 4.20 (q, $J$ = 7.2 Hz, 2H), 6.07 (d, $J$ = 15.6 Hz, 1H), 6.93 (dt, $J$ = 15.6 Hz, 7.2 Hz, 1H). The $N^{\alpha}$-deblocked product was then coupled with Ac-Ser($^t$Bu)-Ala-Val-Leu-OH, and the product was treated with TFA as above to yield **9** showing a single peak on analytical HPLC: $R_t$ 13.84 min ($CH_3CN$ gradient; 20−45% in 30 min). MALDI TOF-MS. Calcd, 677.385 for $C_{31}H_{54}N_6O_9Na$; found, 677.149 for $[M + Na]^+$.

**Ac-Ser-Ala-Val-Leu-NHCH[$CH_2CH_2CON(CH_3)_2$]$CH_2CH_2$CH=CHCOO$C_2H_5$ (11).** This compound was prepared similarly through the homologation of **6** by a Wittig reaction using methoxymethyltriphenylphosphonium chloride followed by a reaction with triethyl phosphonoacetate to yield **8** and coupling with the tetrapeptide: $R_t$ 17.64 min ($CH_3CN$ gradient; 20−40% in 30 min). MALDI TOF-MS. Calcd, 691.401 for $C_{32}H_{56}N_6O_9Na$; found, 691.344 for $[M + Na]^+$.

**Solid-Phase Synthesis of the $P_1$ Site-Substituted Peptide Aldehyde Ac-Ser-Ala-Val-Leu-$P_1$-H.** The peptide aldehyde was synthesized using the Weinreb AM resin (Novabiochem, Merck) according to published procedures,[29] and the product was purified by semipreparative HPLC using Cosmosil 5C18 (10 mm × 250 mm) to afford a white powder with a single chromatographic peak. Ac-Ser-Ala-Val-Leu-Leu-H **11**: yield, 0.8%; $R_t$ 14.76 min ($CH_3CN$ gradient; 20−50% in 30 min). MALDI TOF-MS. Calcd, 550.322 for $C_{25}H_{45}N_5O_7Na$; found, 550.249 for $[M + Na]^+$. Ac-Ser-Ala-Val-Leu-$^t$Bu-Gly-H **12**: yield, 0.5%; $R_t$ 17.46 min ($CH_3CN$ gradient; 20−40% in 30 min). MALDI TOF-MS. Calcd, 550.322 for $C_{25}H_{45}N_5O_7Na$; found, 550.254 for $[M + Na]^+$. Ac-Ser-Ala-Val-Leu-Phe-H **13**: yield, 1.0%; $R_t$ 16.42 min ($CH_3CN$ gradient; 20−50% in 30 min). MALDI TOF-MS. Calcd, 584.306 for $C_{28}H_{43}N_5O_7Na$; found, 584.230 for $[M + Na]^+$. Ac-Ser-Ala-Val-Leu-Cha-H **14**: yield, 0.5%; $R_t$ 19.55 min ($CH_3CN$ gradient; 20−50% in 30 min). MALDI TOF-MS. Calcd, 590.353 for $C_{28}H_{49}N_5O_7Na$; found, 590.310 for $[M + Na]^+$. Ac-Ser-Ala-Val-Leu-Thi-H **15**: yield, 0.5%; $R_t$ 12.30 min ($CH_3CN$ gradient; 20−50% in 30 min). MALDI TOF-MS. Calcd, 590.262 for $C_{26}H_{41}N_5O_7S_1Na$; found, 590.263 for $[M + Na]^+$. Ac-Ser-Ala-Val-Leu-His-H **16**: yield, 4.4%; $R_t$ 12.04 min ($CH_3CN$ gradient; 15−30% in 30 min). MALDI TOF-MS. Calcd, 574.297 for $C_{25}H_{41}N_7O_7Na$; found, 574.258 for $[M + Na]^+$.

**9,10-Epoxydecan-1-ol (17).** To a solution of 9-decen-1-ol (2.0 g, 12 mmol) in $CH_2Cl_2$ (40 mL) was added *m*CPBA (2.4 g, 14 mmol) at 25 °C. After 30 min of stirring, saturated aqueous $Na_2S_2O_3$ (20 mL) and saturated $NaHCO_3$(aq) (20 mL) were added. The organic layer was washed with $H_2O$ and brine, dried over $MgSO_4$, filtered, and concentrated in vacuo. The residue was purified by silica gel column chromatography using hexane:AcOEt (2:1, v/v) to give 1.5 g (64%) of **17** as a colorless oil. $^1$H NMR (500 MHz, $CDCl_3$): $\delta$ 1.33 (brs, 8H), 1.46−1.56 (m, 6H), 2.46 (dd, $J$ = 5.0 Hz, 3.0 Hz, 1H), 2.74 (t, $J$ = 5.0 Hz, 1H), 2.90 (m, 1H), 3.56 (t, $J$ = 6.5 Hz, 2H), 3.89 (brs, 1H). $^{13}$C NMR (125 MHz, $CDCl_3$): $\delta$ 25.3, 25.4, 28.8, 29.0, 31.9, 32.1, 46.6, 51.9, 61.7. IR (film) $\nu_{max}$ cm$^{-1}$: 3408, 3046, 1465, 1056, 833. ESIHRMS $[M + Na]^+$ calcd for $C_{10}H_{20}O_2Na$, 195.1361; found, 195.1308.

**Decan-1,2,10-triol (18).** 9,10-Epoxydecan-1-ol **17** (1.5 g, 7.5 mmol) in THF:1 M NaOH (1:1, 20 mL) was refluxed for 2 h. After it was cooled to room temperature, the mixture was extracted with AcOEt. The organic layer was washed with brine, dried over $MgSO_4$, filtered, and concentrated in vacuo. The residue was purified by silica gel column chromatography using AcOEt:MeOH (4:1, v/v) to give 0.7 g (43%) of decan-1,2,10-triol **18** as a white solid; mp 58−64 °C. $^1$H NMR (500 MHz, $CD_3OD$): $\delta$ 1.32 (brs, 10H), 1.46−1.57 (m, 4H), 3.39 (dd, $J$ = 11.5 Hz, 6.5 Hz, 1H), 3.44 (dd, $J$ = 11.5 Hz, 4.5 Hz, 1H), 3.52 (t, $J$ = 6.5 Hz, 2H), 3.55 (m, 1H). $^{13}$C NMR (125 MHz, $CD_3OD$): $\delta$ 25.4, 25.6, 29.3, 29.4, 29.5, 32.3, 33.1, 61.7, 66.1, 71.9. IR (KBr) $\nu_{max}$ cm$^{-1}$: 3285, 2900, 1468, 1327, 1057, 1020, 965, 878. ESIHRMS $[M + Na]^+$ calcd for $C_{10}H_{22}O_3Na$, 213.1467; found, 213.1455.

**Fmoc-His(Trt)-al.** HN(OMe)Me HCl salt (0.26 g, 2.7 mmol), BOP (1.2 g, 2.7 mmol), and DIEA (1.3 mL, 8.2 mmol) were added to Fmoc-His(Trt)-OH in DMF (10 mL), and the mixture was stirred at 25 °C for 90 min. The solvent was evaporated, and the residue was dissolved in AcOEt. The organic phase was washed with 5% citric acid, 5% $NaHCO_3$, and brine and then dried over $MgSO_4$. The solvent was evaporated to afford 1.6 g (98%) of the corresponding Weinreb amide as a white amorphous powder. $^1$H NMR (300 MHz, $CDCl_3$): $\delta$ 3.01 (brdd, $J$ = 8.7 Hz, 5.1 Hz, 2H), 3.15 (s, 3H), 3.76 (s, 3H), 4.19 (t, $J$ = 7.2 Hz, 1H), 4.29 (d, $J$ = 7.2 Hz, 2H), 4.96 (brdd, $J$ = 8.1 Hz, 5.1 Hz, 1H), 6.14 (brd, $J$ = 8.1 Hz, 1H), 6.58 (s, 1H), 7.10−7.75 (m, 24H). $^{13}$C NMR: $\delta$ 31.00, 32.54, 47.48, 52.00, 61.98, 67.40, 75.52, 119.91, 120.18, 125.62, 127.37, 127.91, 128.32, 130.06, 130.15, 136.73, 138.98, 141.54, 142.29, 144.39, 156.43, 162.64. The product (0.66 g, 10 mmol), without further purification, was dissolved in THF (10 mL), and $LiAlH_4$ (50 mg) was added. The mixture was stirred at 25 °C for 10 min, filtered, and evaporated. The residue was dissolved in $CHCl_3$, and the organic phase was washed with $H_2O$ and dried over $MgSO_4$.

The solvent was removed by evaporation, and the residue was purified by flash chromatography using hexane:AcOEt (1:2 v/v) to yield the desired product as an oil. Yield, 0.50 g (42%); $[\alpha]_D^{26}$ +18.2 (*c* 0.6, $CHCl_3$). $^1$H NMR (300 MHz, $CDCl_3$): $\delta$ 3.05 (dd, *J* = 15.0 Hz, 5.4 Hz, 1H), 3.16 (dd, *J* = 15.0 Hz, 5.4 Hz, 1H), 4.22 (t, *J* = 7.5 Hz, 1H), 4.97 (d, *J* = 7.5 Hz, 2H), 4.46 (dd, *J* = 6.9 Hz, 5.4 Hz, 1H), 6.45 (brd, *J* = 6.9 Hz, 1H), 6.62 (s, 1H), 7.08−7.77 (m, 24H), 9.68 (brs). $^{13}$C NMR: $\delta$ 27.24, 47.21, 59.89, 67.20, 75.37, 119.70, 119.85, 119.96, 125.24, 127.08, 127.54, 127.69, 128.02, 128.09, 128.13, 129.71, 135.88, 138.82, 141.29, 142,27, 142,47, 143.89, 156.39, 200.31.

**Fmoc-His(Trt)-al 1-Octanol-ethylene Acetal [Fmoc-His(Trt)-acetal] (19).** To a stirred solution of Fmoc-His(Trt)-al (0.59 g, 0.98 mmol) and decane-1, 2, 10-triol **18** (0.19 g, 0.98 mmol) in $CH_2Cl_2$ (10 mL) was added $BF_3$-$Et_2O$ (0.2 mL), and the mixture was stirred at 25 °C for 30 min. $H_2O$ (10 mL) was added, and the organic phase was washed with $H_2O$ and dried on $MgSO_4$. The solvent was evaporated to yield 0.57 g (75%) of a white amorphous powder, and the product was used for the next reaction without further purification: $[\alpha]_D^{27}$ −6.3 (*c* 0.8, $CHCl_3$). $^1$H NMR (300 MHz, $CDCl_3$): $\delta$ 1.26−1.30 (m, 12H), 1.49−1.56 (m, 2H), 2.81−2.89 (m, 2H), 3.41−3.51 (m, 1H), 3.57−3.63 (m, 2H), 3.92−4.06 (m, 2H), 4.11−4.29 (m, 4H), 4.98−5.04 (m, 1H), 5.43−5.57 (m, 1H), 6.68 (s, 1H), 7.06−7.75 (m, 24H). $^{13}$C NMR: $\delta$ 25.71, 25.84, 28.68, 29.35, 29.44, 29.52, 32.88, 33.25, 47.42, 53.42, 62.86, 67.09, 70.27, 75.38, 103.98, 120.02, 125.44, 127.19, 127.74, 128.00, 128.15, 128.87, 129.92, 137.77, 138.49, 141.38, 142.59, 144.20, 156.52, 162.49.

**Solid-Phase Synthesis of the Peptide Thioacetal [Ac-Ala-Val-Cha-His-(SEt)$_2$] (22).** To a stirred solution of **19** (0.37 g, 0.48 mmol) in acetone (5 mL) was added Jones reagent (0.3 mL; 2.67 M solution) at 0 °C, and the mixture was stirred for 40 min at 25 °C. 2-Propanol (0.1 mL) was then added, and the mixture was filtered through a Celite pad. The solvent was removed by evaporation, and the residue was extracted with $CHCl_3$. The organic layer was washed with $H_2O$, dried over $MgSO_4$, and evaporated to yield 0.30 g (80%) of the corresponding carboxylic acid **20** as an amorphous powder: $[\alpha]_D^{27}$ −13.1 (*c* 0.8, $CHCl_3$). $^1$H NMR (300 MHz, $CDCl_3$): $\delta$ 1.26−1.58 (m, 12H), 2.31−2.41 (m, 2H), 2.86−2.95 (m, 2H), 3.45−3.52 (m, 1H), 3.95 (t, *J* = 6.9 Hz, 1H), 4.06−4.38 (m, 6H), 5.06 (d, *J* = 7.2 Hz, 1H), 6.69 (s, 1H), 6.99−7.74 (m, 24H). $^{13}$C NMR: $\delta$ 24.80, 28.93, 29.24, 34.32, 46.58, 47.15, 53.77, 66.85, 119.91, 125.29, 127.06, 127.66, 128.11, 128.23, 128.32, 128.47, 129.63, 141.20, 143.78, 155.60, 181.82. The product was used without further purification.

Piperidine (20%) in DMF (3 mL) was added to a DMF-swelled Rink amide resin [4-(2,4-dimethoxyphenyl-Fmoc-aminomethyl)-phenoxy resin] (140 mg, 89 $\mu$mol), and the mixture was agitated at 25 °C for 20 min. The resin was washed with DMF, the above carboxylic acid **20** (0.28 g, 0.35 mmol), HOBt (54 mg, 0.35 mmol), DIEA (170 $\mu$L, 1.1 mmol), and DIPCDI (62 $\mu$L, 0.35 mmol) in DMF (2 mL) were added, and the mixture was agitated at 25 °C for 10 h. Deprotection of the $N^{\alpha}$-Fmoc group by treatment with 20% piperidine in DMF and coupling with $N^{\alpha}$-Fmoc-$\beta$-cyclohexyl-L-alanin (Fmoc-Cha-OH) (170 mg, 0.44 mmol) using DIPCDI/HOBt were carried out as above. An aliquot of the resulting resin [Fmoc-Cha-His(Trt)-acetal resin] (0.10 g, 40 $\mu$mol) was then used for coupling with Fmoc-Val-OH (68 mg, 0.20 mmol) and Fmoc-Ala-OH (62 mg, 0.20 mmol) and acetylation using $Ac_2O$ (76 $\mu$L, 0.80 mmol) and DIEA (130 $\mu$L, 0.80 mmol) to afford the Ac-Ala-Val-Cha-His(Trt)-acetal resin. To the dried resin were added anisole (87 $\mu$L, 0.80 mmol) and TFA (1.5 mL), and the mixture was agitated at 25 °C for 4 h. The mixture was filtered, and the solvent was removed by evaporation. Ether and $H_2O$ were added to the residue, and the aqueous phase was washed with ether. The solvent was removed by lyophilization to afford **21** as a powder: MALDI-TOF MS. Calcd, 690.456 for $C_{35}H_{60}N_7O_7$; found, 690.302 for $[M + H]^+$.

To the crude product in AcOH (1 mL) were added ethanethiol (0.13 mL, 1.8 mmol) and $BF_3$-$Et_2O$ (100 $\mu$L). The mixture was stirred at 25 °C for 2 h, and $H_2O$ (400 $\mu$L) was added. Then, 150 $\mu$L of the solution was applied to a semipreparative HPLC column (Cosmosil 5C18, 10 mm × 250 mm) and eluted with a gradient of $CH_3CN$ (10−60%, 60 min) in 0.1% aqueous TFA at 3 mL/min. The desired thioacetal **22** eluted at 43.60 min. The rest of the solution was similarly purified and lyophilized to yield 20 mg (82%) of **22** as a white powder. $^1$H NMR (300 MHz, $D_2O$): $\delta$ 1.11 (d, *J* = 6.6 Hz, 3H), 1.15 (d, *J* = 6.6 Hz, 3H), 1.20−1.23 (m, 2H), 1.47−1.66 (m, 4H), 1.55 (t, *J* = 7.5 Hz, 3H), 1.56 (t, *J* = 7.5 Hz, 3H), 1.61 (d, *J* = 7.2 Hz, 3H), 1.80−1.98 (m, 7H), 2.28 (s, 3H), 2.30−2.33 (m, 1H), 3.01 (q, *J* = 7.5 Hz, 2H), 3.03 (q, *J* = 7.5 Hz, 2H), 3.32 (dd, *J* = 15.3 Hz, 10.8 Hz, 1H), 3.58 (dd, *J* = 15.3 Hz, 3.6 Hz, 1H), 4.32 (d, *J* = 4.8 Hz, 1H), 4.37 (d, *J* = 7.5 Hz, 1H), 4.57−4.64 (m, 2H), 4.71−4.75 (m, 1H), 7.55 (s, 1H), 8,84 (s, 1H). $^{13}$C NMR: $\delta$ 14.18, 14.34, 16.99, 17.84, 18.79, 22.10, 25.98, 26.06, 26.15, 26.25, 26.44, 27.04, 30.69, 32.46, 33.36, 33.87, 39.33, 49.99, 51.67, 52.43, 54.88, 59.26, 117.30, 130.23, 133.66, 172.63, 173.72, 173.75, 174.88. MALDI-TOF MS. Calcd, 633.324 for $C_{29}H_{50}N_6O_4S_2Na$; found, 633.299 for $[M + Na]^+$. Peptide thioacetals **23**−**27** were similarly prepared as above.

**Ac-Asn-Val-Cha-His-(SEt)$_2$ (23).** Yield, 74%. $^1$H NMR (300 MHz, $D_2O$): $\delta$ 0.99 (d, *J* = 6.9 Hz, 3H), 1.01 (d, *J* = 6.9 Hz, 3H), 1.00−1.12 (m, 2H), 1.33−1.56 (m, 4H), 1.43 (t, *J* = 7.5 Hz, 3H), 1.44 (t, *J* = 7.5 Hz, 3H), 1.67−1.92 (m, 7H), 2.18 (s, 3H), 2.18−2.22 (m, 1H), 2.78−2.96 (m, 4H), 3.31 (dd, *J* = 15.6 Hz, 10.8 Hz, 1H), 3.46 (dd, *J* = 15.3 Hz, 3.3 Hz, 1H), 4.21 (d, *J* = 5.1 Hz, 1H), 4.28 (d, *J* = 6.9 Hz, 1H), 4.45−4.50 (m, 1H), 4.60−4.65 (m, 1H), 4.86 (brt, *J* = 6.9 Hz, 1H), 7.43 (s, 1H), 8,74 (s, 1H). $^{13}$C NMR: $\delta$ 14.05, 14.23, 17.47, 18.65, 22.05, 25.85, 25.95, 26.02, 26.14, 26.32, 26.88, 30.60, 32.34, 33.18, 33.69, 36.44, 39.00, 50.67, 51.65, 52.25, 54.65, 59.17, 114.88, 130.00, 133.51, 172.53, 172.54, 173.80, 173.81, 174.36. MALDI-TOF MS. Calcd, 654.347 for $C_{30}H_{52}N_7O_5S_2$; found, 654.442 for $[M + H]^+$.

**Ac-Ser-Val-Cha-His-(SEt)$_2$ (24).** Yield, 21%. $^1$H NMR (300 MHz, $D_2O$): $\delta$ 0.84 (d, *J* = 6.9 Hz, 3H), 0.89 (d, *J* = 6.9 Hz, 3H), 0.90−1.00 (m, 2H), 1.15−1.36 (m, 4H), 1.27 (t, *J* = 7.5 Hz, 3H), 1.29 (t, *J* = 7.5 Hz, 3H), 1.54−1.69 (m, 7H), 2.03−2.10 (m, 1H), 2.06 (s, 3H), 2.746 (q, *J* = 7.5 Hz, 2H), 2.753 (q, *J* = 7.5 Hz, 2H), 3.07 (dd, *J* = 15.6 Hz, 11.1 Hz, 1H), 3.31 (dd, *J* = 15.6 Hz, 3.0 Hz, 1H), 3.81 (d, *J* = 6.3 Hz, 1H), 4.08 (d, *J* = 4.8 Hz, 1H), 4.13 (d, *J* = 7.2 Hz, 1H), 4.34 (dd, *J* = 9.0 Hz, 6.3 Hz, 1H), 4.43−4.53 (m, 2H), 7.26 (s, 1H), 8,55 (s, 1H). $^{13}$C NMR: $\delta$ 13.82, 14.01, 17.49, 18.44, 21.84, 25.72, 25.80, 25.86, 26.06, 26.20, 26.86, 30.17, 32.05, 32.94, 33.51, 38.90, 51.52, 52.23, 54.34, 55.62, 59.23, 61.20, 116.93, 130.04, 133.43, 171.97, 172.61, 174.05, 174.35. MALDI-TOF MS. Calcd, 627.336 for $C_{29}H_{51}N_6O_5S_2$; found, 627.332 for $[M + H]^+$.

**Ac-Ser(Ac)-Val-Cha-His-(SEt)$_2$ (28).** $^1$H NMR (300 MHz, $D_2O$): $\delta$ 0.82 (d, *J* = 6.6 Hz, 3H), 0.89 (d, *J* = 6.6 Hz, 3H), 0.91−0.96 (m, 2H), 1.18−1.35 (m, 4H), 1.27 (t, *J* = 7.5 Hz, 3H), 1.29 (t, *J* = 7.5 Hz, 3H), 1.55−1.69 (m, 7H), 2.04−2.10 (m, 1H), 2.07 (s, 3H), 2.10 (s, 3H), 2.746 (q, *J* = 7.5 Hz, 2H), 2.755 (q, *J* = 7.5 Hz, 2H), 3.09 (dd, *J* = 15.3 Hz, 10.8 Hz, 1H), 3.32 (dd, *J* = 15.3 Hz, 3.3 Hz, 1H), 4.09 (d, *J* = 4.5 Hz, 1H), 4.11 (d, *J* = 7.5 Hz, 1H), 4.27−4.42 (m, 3H), 4.50−4.54 (m, 1H), 7.28 (s, 1H), 8,60 (s, 1H). $^{13}$C NMR: $\delta$ 13.82, 14.02, 17.73, 18.46, 20.28, 21.81, 25.74, 25.80, 25.85, 26.06, 26.20, 26.80, 30.36, 32.10, 32.95, 33.53, 38.99, 51.51, 52.18, 52.73, 54.37, 59.28, 63.44, 116.94, 129.89, 130.05, 133.33, 170.68, 172.31, 173.47, 173.99, 174.27. MALDI-TOF MS. Calcd, 669.347 for $C_{31}H_{53}N_6O_6S_2$; found, 669.348 for $[M + H]^+$.

**Ac-Thr-Val-Cha-His-(SEt)$_2$ (25).** Yield, 31%. $^1$H NMR (300 MHz, $D_2O$): $\delta$ 0.75 (d, *J* = 6.6 Hz, 3H), 0.85 (d, *J* = 6.6 Hz, 3H), 0.84−0.95 (m, 2H), 1.11−1.30 (m, 4H), 1.13 (d, *J* = 6.6 Hz, 3H), 1.22 (t, *J* = 7.5 Hz, 3H), 1.23 (t, *J* = 7.5 Hz, 3H), 1.48−1.60 (m, 7H), 1.98−2.02 (m, 1H), 2.02 (s, 3H), 2.69 (q, *J* = 7.5 Hz, 2H), 2.70 (q, *J* = 7.5 Hz, 2H), 3.03 (dd, *J* = 15.3 Hz, 11.1 Hz, 1H), 3.26 (dd, *J* = 15.3 Hz, 3.0 Hz, 1H), 4.01−4.08 (m, 3H), 4.22 (d, *J* = 5.7 Hz, 1H), 4.28−4.32 (m, 1H), 4.43−4.50 (m, 1H), 7.22 (s, 1H), 8,54 (s, 1H). $^{13}$C NMR: $\delta$ 13.76, 13.94, 17.73, 18.37, 18.88, 21.76, 25.67, 25.76, 25.80, 26.00, 26.16, 26.74, 38.91, 51.35, 52.12, 54.27, 59.23, 59.49, 67.04, 119.88, 129.79, 133.23, 171.74, 172,45, 174.02, 174.38. MALDI-TOF MS. Calcd, 641.352 for $C_{30}H_{53}N_6O_5S_2$; found, 641.283 for $[M + H]^+$.

**Ac-Ser-Ala-Val-Phe-His-(SEt)$_2$ (26).** Yield, 18%. $^1$H NMR (300 MHz, $D_2O$): $\delta$ 0.65 (d, *J* = 6.6 Hz, 3H), 0.76 (d, *J* = 6.6 Hz, 3H), 1.15 (t, *J* = 7.5 Hz, 3H), 1.20 (t, *J* = 7.5 Hz, 3H), 1.26 (d, *J* = 7.2 Hz, 3H), 1.77−1.86 (m, 1H), 2.00 (s, 3H), 2.55 (q, J *J* = 7.5 Hz, 2H), 2.64 (q, *J* = 7.5 Hz, 2H), 2.85−2.95 (m, 2H), 3.01 (dd, *J* = 15.3 Hz, 7.5 Hz, 1H), 3.21 (dd, *J* = 15.3 Hz, 3.0 Hz, 1H), 3.67 (d, *J* = 4.2 Hz, 1H),

3.770 (d, $J$ = 5.7 Hz, 1H), 3.775 (d, $J$ = 5.7 Hz, 1H), 3.91 (d, $J$ = 7.8 Hz, 1H), 4.23−4.43 (m, 3H), 4.53 (brt, $J$ = 8.0 Hz, 1H), 7.12−7.33 (m, 61H), 8.45 (s, 1H). $^{13}$C NMR: $\delta$ 13.68, 13.94, 16.45, 17.71, 18.26, 21.78, 26.10, 26.32, 30.19, 37.41, 49.65, 52.33, 54.30, 54.62, 55.67, 59.32, 61.14, 116.86, 127.30, 128.84, 129.23, 130.02, 133.40, 136.15, 171.91, 172.36, 172.56, 174.53, 174.58. MALDI-TOF MS. Calcd, 692.327 for $C_{32}H_{50}N_7O_6S_2$; found, 692.475 for $[M + H]^+$.

**Ac-Ser-Ala-Val-Cha-His-(SEt)$_2$ (27).** Yield, 17%. $^1$H NMR (300 MHz, $D_2O$): $\delta$ 0.75 (d, $J$ = 6.6 Hz, 3H), 0.84 (d, $J$ = 6.6 Hz, 3H), 0.85−0.94 (m, 2H), 1.08−1.33 (m, 4H), 1.20 (t, $J$ = 7.5 Hz, 3H), 1.22 (t, $J$ = 7.5 Hz, 3H), 1.32 (d, $J$ = 7.2 Hz, 3H), 1.42−1.58 (m, 7H), 1.88−2.01 (m, 1H), 2.01 (s, 3H), 2.68 (q, $J$ = 7.5 Hz, 2H), 2.69 (q, $J$ = 7.5 Hz, 2H), 3.03 (dd, $J$ = 15.3 Hz, 10.8 Hz, 1H), 3.26 (dd, $J$ = 15.3 Hz, 3.3 Hz, 1H), 3.74−3.84 (m, 2H), 3.96 (d, $J$ = 8.1 Hz, 1H), 4.04 (d, $J$ = 4.5 Hz, 1H), 4.26−4.36 (m, 3H), 4.43−4.49 (m, 1H), 7.20 (s, 1H), 8.50 (s, 1H). $^{13}$C NMR: $\delta$ 13.69, 13.88, 16.45, 17.73, 18.36, 21.75, 25.64, 25.73, 25.85, 25.97, 26.20, 26.79, 29.97, 31.88, 32.87, 33.41, 38.84, 49.75, 51.44, 52.22, 54.25, 55.72, 59.41, 61.11, 116.85, 129.87, 133.27, 171.98, 172.72, 174.22, 174.58, 174.66. MALDI-TOF MS. Calcd, 698.374 for $C_{32}H_{56}N_7O_6S_2$; found, 698.389 for $[M + H]^+$.

**Ac-Ser(Ac)-Ala-Val-Cha-His-(SEt)$_2$ (29).** $^1$H NMR (300 MHz, $D_2O$): $\delta$ 0.91 (d, $J$ = 6.6 Hz, 3H), 0.97 (d, $J$ = 6.6 Hz, 3H), 0.98−1.09 (m, 2H), 1.24−1.51 (m, 4H), 1.36 (t, $J$ = 7.5 Hz, 3H), 1.37 (t, $J$ = 7.5 Hz, 3H), 1.45 (d, $J$ = 7.2 Hz, 3H), 1.59−1.75 (m, 7H), 2.11−2.16 (m, 1H), 2.15 (s, 3H), 2.19 (s, 3H), 2.83 (q, $J$ = 7.5 Hz, 2H), 2.84 (q, $J$ = 7.5 Hz, 2H), 3.15 (dd, $J$ = 15.6 Hz, 10.8 Hz, 1H), 3.40 (dd, $J$ = 15.3 Hz, 3.3 Hz, 1H), 4.13−4.18 (m, 2H), 4.40−4.51 (m, 4H), 4.54−4.61 (m, 1H), 7.36 (s, 1H), 8.66 (s, 1H). $^{13}$C NMR: $\delta$ 13.95, 14.13, 16.72, 17.78, 18.58, 20.34, 21.98, 25.84, 25.93, 26.14, 26.82, 30.37, 32.15, 33.12, 33.59, 39.08, 49.86, 51.53, 52.23, 53.04, 54.49, 59.26, 63.52, 117.02, 129.95, 132.42, 170.72, 172.58, 173.47, 173.89, 174.13, 174.29. MALDI-TOF MS. Calcd, 740.384 for $C_{34}H_{58}N_7O_7S_2$; found, 740.190 for $[M + H]^+$.

**Ac-Ala-Val-Cha-His-H (32).** Ac-Ala-Val-Cha-His-(SEt)$_2$ **22** (9.0 mg, 15 $\mu$mol) was dissolved in $H_2O$:THF(2:1, 1.35 mL). A 150 $\mu$L amount of the solution was mixed with 53 $\mu$L of a 0.1 mmol/L THF solution of NBS, and the mixture was applied to a semipreparative HPLC column (Cosmosil 5C18, 10 mm × 250 mm). The desired product was eluted with a gradient of $CH_3CN$ (10−60%, 60 min) in 0.1% aqueous TFA at 3 mL/min, appearing at 23.26 min. The rest of the solution was similarly purified and lyophilized to yield 3.2 mg (43%) of **32** as a white powder: $R_t$ on analytical HPLC, 12.87 min (single peak). $^1$H NMR (300 MHz, $D_2O$): $\delta$ 0.78 (d, $J$ = 6.9 Hz, 3H), 0.84−0.94 (m, 2H), 0.86 (d, $J$ = 6.9 Hz, 3H), 1.05−1.25 (m, 5H), 1.30 (d, $J$ = 7.2 Hz, 3H), 1.39−1.58 (m, 6H), 1.91−2.02 (m, 1H), 1.97 (s, 3H), 2.84 (dd, $J$ = 15.3 Hz, 10.8 Hz, 1H), 3.11 (dd, $J$ = 15.3 Hz, 3.3 Hz, 1H), 4.00 (d, $J$ = 8.1 Hz, 1H), 4.06−4.11 (m, 1H), 4.20−4.31 (m, 2H), 7.21 (s, 1H), 8.53 (s, 1H), 9.51 (brs). MALDI-TOF MS. Calcd, 505.314 for $C_{25}H_{41}N_6O_5$; found, 505.353 for $[M + H]^+$. The following peptidealdehydes were similarly prepared as above.

**Ac-Asn-Val-Cha-His-H (33).** Yield, 51%; $R_t$ on analytical HPLC, 12.35 min (single peak). $^1$H NMR (300 MHz, $D_2O$): $\delta$ 0.89−0.96 (m, 8H), 1.10−1.26 (m, 4H), 1.44−1.64 (m, 7H), 1.98 (s, 3H), 2.16−2.20 (m, 1H), 2.71−2.81 (m, 3H), 2.93−2.98 (m, 1H), 3.98−4.02 (m, 2H), 4.15−4.20 (m, 1H), 4.61−4.64 (m, 1H), 7.18 (s, 1H), 8.46 (s, 1H), 9.44 (brs). MALDI-TOF MS. Calcd, 548.320 for $C_{26}H_{42}N_7O_6$; found, 548.375 for $[M + H]^+$.

**Ac-Ser-Val-Cha-His-H (34).** Yield, 60%; $R_t$ on analytical HPLC, 13.11 min (single peak). $^1$H NMR (300 MHz, $D_2O$): $\delta$ 0.69−1.10 (m, 6H), 0.72 (d, $J$ = 6.9 Hz, 3H), 0.77 (d, $J$ = 6.9 Hz, 3H), 1.28−1.49 (m, 7H), 1.87−1.94 (m, 1H), 1.94 (s, 3H), 2.76 (dd, $J$ = 15.3 Hz, 10.8 Hz, 1H), 3.03 (dd, $J$ = 15.3 Hz, 3.3 Hz, 1H), 3.66−3.73 (m, 2H), 3.96−4.04 (m, 2H), 4.12−4.21 (m, 1H), 4.30−4.34 (m, 1H), 7.12 (brs, 1H), 8.46 (brs, 1H), 9.42 (brs). MALDI-TOF MS. Calcd, 521.309 for $C_{25}H_{41}N_6O_6$; found, 521.329 for $[M + H]^+$.

**Ac-Thr-Val-Cha-His-H (35).** Yield, 40%; $R_t$ on analytical HPLC, 12.27 min (single peak). $^1$H NMR (300 MHz, $D_2O$): $\delta$ 0.89−0.93 (m, 8H), 1.11−1.24 (m, 7H), 1.41−1.63 (m, 7H), 2.03 (s, 3H), 2.11−2.18 (m, 1H), 3.01−3.08 (m, 1H), 3.24−3.31 (m, 1H), 4.02−4.05 (m, 1H), 4.13−4.25 (m, 3H), 4.37−4.41 (m, 1H), 7.21 (brs, 1H), 8.44 (brs, 1H), 9.44 (brs). MALDI-TOF MS. Calcd, 535.324 for $C_{26}H_{43}N_6O_6$; found, 535.383 for $[M + H]^+$.

**Ac-Ser-Ala-Val-Phe-His-H (30).** Yield, 12%; $R_t$ on analytical HPLC, 10.27 min (single peak). $^1$H NMR (300 MHz, $D_2O$): $\delta$ 0.66 (d, $J$ = 6.6 Hz, 3H), 0.76 (d, $J$ = 6.6 Hz, 3H), 1.26 (d, $J$ = 7.2 Hz, 3H), 1.79−1.89 (m, 1H), 2.00 (s, 3H), 2.76 (dd, $J$ = 15.6 Hz, 11.1 Hz, 1H), 2.85−2.99 (m, 2H), 3.04 (dd, $J$ = 15.6 Hz, 3.0 Hz, 1H), 3.724−3.82 (m, 2H), 3.91 (d, $J$ = 8.1 Hz, 1H), 3.99−4.04 (m, 1H), 4.27 (q, $J$ = 7.2 Hz, 1H), 4.34 (t, $J$ = 5.7 Hz, 1H), 4.51 (brt, $J$ = 7.2 Hz, 1H), 7.15−7.31 (m, 6H), 8.48 (brs, 1H). MALDI-TOF MS. Calcd, 586.299 for $C_{28}H_{40}N_7O_7$; found, 586.380 for $[M + H]^+$.

**Ac-Ser-Ala-Val-Cha-His-H (31).** Yield, 46%; $R_t$ on analytical HPLC, 12.66 min (single peak). $^1$H NMR (300 MHz, $D_2O$): $\delta$ 0.78 (d, $J$ = 6.6 Hz, 3H), 0.79−0.93 (m, 2H), 0.85 (d, $J$ = 6.6 Hz, 3H), 1.00−1.24 (m, 5H), 1.33 (d, $J$ = 7.2 Hz, 3H), 1.42−1.59 (m, 6H), 1.89−2.01 (m, 1H), 2.01 (s, 3H), 2.79 (dd, $J$ = 15.6 Hz, 10.8 Hz, 1H), 3.06 (dd, $J$ = 15.6 Hz, 3.6 Hz, 1H), 3.74−3.81 (m, 2H), 3.96 (d, $J$ = 8.1 Hz, 1H), 4.03−4.09 (m, 1H), 4.25−4.37 (m, 3H), 7.10 (s, 1H), 8.28 (s, 1H), 9.47 (brs). MALDI-TOF MS. Calcd, 592.346 for $C_{28}H_{46}N_7O_7$; found, 592.435 for $[M + H]^+$.

**X-ray Crystallography.** Prior to the crystallization of the inhibitor complex, the purified R188I mutant SARS 3CL protease in 20 mM Bis-Tris, pH 5.5/100 mM NaCl/5 mM DTT (8 mg/mL) was crystallized at 4 °C using the sitting drop vapor diffusion method by mixing it with an equal volume of a precipitant solution (9−11% (w/v) of PEG20000, 100 mM MES, pH 6.0, and 5 mM DTT). Diffraction-quality crystals were formed within 3 days and reached a typical size of 0.3 mm × 0.3 mm × 0.2 mm.

For crystallization of the inhibitor complex, the R188I SARS 3CL protease solution (8 mg/mL) was mixed with the inhibitor dissolved in DMSO at a molar ratio of 1:4 and then incubated for 1 h at 4 °C before being combined with an equal volume of the precipitant solution described above. The crystal form of the inhibitor complex was then transferred to a cryoprotectant solution of 11% PEG20000, 100 mM MES, pH 6.0, 5 mM DTT, and 15% (v/v) ethylene glycol and flash-frozen in a liquid nitrogen stream prior to the collection of X-ray diffraction data.

X-ray data were collected from frozen crystals at 95 K at the Photon Factory (Tsukuba, Japan). Diffraction data were collected from a crystal of the R188I SARS 3CL protease on a beamline BL-5A with an ADSC Quantum 315r CCD detector at a wavelength of 1.0000 Å. A data set from a protease crystal in a complex with the inhibitor was collected on a BL-6A on an ADSC Quantum 4r CCD detector at a wavelength of 0.9780 Å. The diffraction data were processed using the HKL-2000 software program.

The structures of the R188I SARS 3CL protease alone and complexed with inhibitors were determined by molecular replacement using the Molrep program with a wild-type SARS 3CL protease structure (PDB code: 2ZU4) as the search model. Rigid body refinement and subsequent restrained refinement protocols were performed with the program Refmac 5 of the CCP package. The Coot program was used for manual model rebuilding. Water molecules were added using Coot only after the refinement of protein structures had converged. Ligands were directly built into the corresponding difference electron density, and the model was then subjected to an additional round of refinement.

**Estimation of IC$_{50}$ Values.** Peptide substrate SO1 [H-Thr-Ser-Ala-Val-Leu-Gln-Ser-Gly-Phe-Arg-Lys-$NH_2$][27] (111 $\mu$M) in a reaction solution (25 $\mu$L of 20 mM Tris-HCl buffer, pH 7.5, containing 7 mM DTT) was incubated with the R188I SARS protease[27] (56 nM) at 37 °C for 60 min in the presence of various inhibitor concentrations. In a preincubation procedure, the mutant protease was incubated with the inhibitor at 37 °C for 20−30 min before addition of the substrate. The substrate was then added to the mixture, and the cleavage reaction was continued for a further 60 min. In a simultaneous mixing procedure, the protease, inhibitor, and substrate were simultaneously mixed, and the mixture was incubated at 37 °C for 60 min. The cleavage reaction was monitored by analytical HPLC [Cosmosil 5C18 column (4.6 mm × 150 mm), a linear gradient of $CH_3CN$ (10−20%) in an aqueous 0.1% TFA over 30 min], and the cleavage rates were calculated from


dx.doi.org/10.1021/jm200870n | J. Med. Chem. 2011, 54, 7962−7973

the decease of the substrate peak area. Each $IC_{50}$ value was obtained from the sigmoidal dose−response curve (see Figure S-1 in the Supporting Information for a typical sigmoidal curve). Each experiment was repeated three times, and the results were averaged.

**Lineweaver−Burk Plot.** Initial rate measurements for the hydrolysis were carried out using basically the same procedure as above. Each reaction was initiated by adding the protease (56 nM) to various solutions containing different final concentrations of the substrate (34−168 $\mu$M) in the absence or presence of **35** (25, 50, or 100 nM). The digestion time (10−15 min) varied depending on the amount of substrate used. After the reaction, each mixture was analyzed by HPLC, as described above. The initial digestion rate ($v$, $\mu$M/min) was calculated from the decrease in the peak area of the substrate, and $1/v$ was plotted vs $1/[S]$, where [S] is the concentration of the substrate ($\mu$M).

## ■ ASSOCIATED CONTENT

### Ⓢ Supporting Information

HPLC data for inhibitors, typical sigmoidal curve used to obtain $IC_{50}$ values, and Lineweaver−Burk plots obtained at different concentrations (0, 25, 50, and 100 nM) of **35**. This material is available free of charge via the Internet at http://pubs.acs.org.

### Accession Codes

PDB codes: 3AW1, 3AW0, 3AVZ, and 3ATW.

## ■ AUTHOR INFORMATION


### Corresponding Author

*Tel: +81-75-595-4635. Fax: +81-75-591-9900. E-mail: akaji@mb.kyoto-phu.ac.jp.


## ■ ACKNOWLEDGMENTS

This work was supported, in part, by a Grant-in-Aid for Scientific Research 21590017 to K.A. from the Japan Society for the Promotion of Science.

## ■ ABBREVIATIONS USED

SARS, severe acute respiratory syndrome; CoV, coronavirus; 3CL, chymotrypsin-like protease; DIPCDI, diisopropylcarbodiimide; HOBt, 1-hydroxybenzotriazole; BOP, benzotriazole-1-yl-oxy-tris-(dimethylamino)-phosphonium hexafluorophosphate; HOOBt, 3-hydroxy-1,2,3-benzotriazine-4-one; WSC, water-soluble carbodiimide

## ■ REFERENCES


(1) Lee, N.; Hui, D.; Wu, A.; Chan, P.; Cameron, P.; Joynt, F. M.; Ahuja, A.; Yung, M. Y.; Leung, C. B.; To, K. F.; Leu, M. D.; Szeto, C. C.; Chung, S.; Sung, J. J. Y. A major outbreak of severe acute respiratory syndrome in Hong Kong. *N. Engl. J. Med.* **2003**, *348*, 1986−1994.

(2) Drosten, C.; Günther, S.; Preiser, W.; Ven der Werf, S.; Brodt, H. R.; Becker, S.; Rabenau, H.; Panning, M.; Kolensnikova, L.; Fouchier, R. A. M.; Berger, A.; Burguière, A. M.; Cinatl, J.; Eickmann, M.; Escriou, N.; Grywna, K.; Kramme, S.; Manuguerra, J.; Müller, S.; Rickerts, V.; Stürmer, M.; Vieth, S.; Klenk, H. D.; Osterhaus, A. D. M. E.; Schmitz, H.; Doerr, H. W. Identification of a novel coronavirus in patients with severe acute respiratory syndrome. *N. Engl. J. Med.* **2003**, *348*, 1967−1976.

(3) Ksiazek, T. G.; Erdman, D.; Goldsmith, C. S.; Zaki, S. R.; Peret, T.; Emery, S.; Tong, S.; Urbani, C.; Comer, J. A.; Lim, W.; Rollin, P. E.; Dowell, S. F.; Ling, A. E.; Humphrey, C. D.; Shieh, W. J.; Guarner, J.; Paddock, C. D.; Rota, P.; Fields, B.; DeRisi, J.; Yang, J. Y.; Cox, N.; Hughes, J. M.; LeDuc, J. W.; Bellini, W. J.; Anderson, L. J. A novel coronavirus associated with severe acute respiratory syndrome. *N. Engl. J. Med.* **2003**, *348*, 1953−1966.

(4) Li, W.; Shi, Z.; Yu, M.; Ren, W.; Smith, C.; Epstein, J. H.; Wang, H.; Crameri, G.; Hu, Z.; Zhang, J.; McEachern, J.; Field, H.; Daszak, P.; Eaton, B. T.; Zhang, S.; Wang, L. F. Bats are natural reservoirs of SARS-like coronaviruses. *Science* **2005**, *310*, 676−679.

(5) Lau, S. K. P.; Woo, P. C. Y.; Li, K. S. M.; Huang, Y.; Tsoi, H. W.; Wong, B. H. L.; Wong, S. S. Y.; Leung, S. Y.; Chan, K. H.; Yuen, K. Y. Severe acute respiratory syndrome coronavirus-like virus in Chinese horseshoe bats. *Proc. Natl. Acad. Sci. U.S.A.* **2005**, *102*, 14040−14045.

(6) Rota, P. A.; Oberste, M. S.; Monroe, S. S.; Nix, W. A.; Campagnoli, R.; Icenogle, J. P.; Penaranda, S.; Bankamp, B.; Maher, K.; Chem, M. H.; Tong, W.; Tamin, A.; Lowe, L.; Frace, M.; DeRisi, J. L.; Chen, Q.; Wang, D.; Erdman, D. D.; Peret, T. C.; Burns, C.; Ksiazek, T. G.; Rollin, P. E.; Sanchez, A.; Liffick, S.; Holloway, B.; Limor, J.; McCaustland, K.; Olsen-Rasmussen, M.; Fouchier, R.; Gunther, S.; Osterhaus, A. D.; Drosten, C.; Pallansch, M. A.; Anderson, L. J.; Bellini, W. J. Characterization of a novel coronavirus associated with severe acute respiratory syndrome. *Science* **2003**, *300*, 1394−1399.

(7) Marra, M. A.; Jones, S. J.; Astell, C. R.; Holt, R. A.; Brooks-Wilson, A.; Butterfield, Y. S.; Khattra, J.; Asano, J. K.; Barber, S. A.; Chan, S. Y.; Cloutier, A.; Coughlin, S. M.; Freeman, D.; Girn, N.; Griffith, O. L.; Leach, S. R.; Mayo, M.; McDonald, H.; Montgomery, S. B.; Pandoh, P. K.; Petrescu, A. S.; Robertson, A. G.; Schein, J. E.; Siddiqui, A.; Smailus, D. E.; Sott, J. M.; Yang, G. S.; Plummer, F.; Andonov, A.; Artsob, H.; Bastien, N.; Bermard, K.; Booth, T. F.; Bowness, D.; Czub, M.; Drebot, M.; Fernando, L.; Flick, R.; Garbutt, M.; Gray, M.; Grolla, A.; Jones, S.; Feldmann, H.; Meyers, A.; Kabani, A.; Li, Y.; Normand, S.; Stroher, U.; Tipples, G. A.; Tyler, S.; Vogrig, R.; Ward, D.; Watson, B.; Brunham, R. C.; Krajden, M.; Petric, M.; Skowronski, D. M.; Upton, C.; Roper, R. L. The genome sequence of the SARS-associated coronavirus. *Science* **2003**, *300*, 1399−1404.

(8) Thiel, V.; Ivanov, K. A.; Putics, Á.; Hertzig, T.; Schelle, B.; Bayer, S.; Weißbrich, B.; Snijder, E. J.; Rabenau, H.; Doerr, H. W.; Gorbalenya, A. E.; Ziebuhr, J. Mechanisms and enzymes involved in SARS coronavirus genome expression. *J. Gen. Viol.* **2003**, *84*, 2305−2315.

(9) Anand, K.; Palm, G. J.; Mesters, J. R.; Siddell, S. G.; Ziebuhr, J.; Hilgenfeld, R. Structure of coronavirus main proteinase reveals combination of a chymotrypsin fold with an extra $\alpha$-helical domain. *EMBO J.* **2002**, *21*, 3213−3224.

(10) Anand, K.; Ziebuhr, J.; Wadhwani, P.; Mesters, J. R.; Hilgenfeld, R. Coronavirus main proteinase ($3CL^{pro}$) structure: Basis for design of anti-SARS drugs. *Science* **2003**, *300*, 1763−1767.

(11) Fan, K.; Wei, P.; Feng, Q.; Chen, S.; Huang, C.; Ma, L.; Lai, B.; Pei, J.; Liu, Y.; Chen, J.; Lai, L. Biosynthesis, purification, and substrate specificity of sever acute respiratory syndrome coronavirus 3C-like proteinase. *J. Biol. Chem.* **2004**, *279*, 1637−1642.

(12) Li, C.; Qi, Y.; Teng, X.; Yang, Z.; Wei, P.; Zhang, C.; Tan, L.; Zhou, L.; Liu, Y.; Lai, L. Maturation mechanism of severe acute respiratory syndrome (SARS) coronavirus 3C-like proteinase. *J. Biol. Chem.* **2010**, *285*, 28134−28140.

(13) Kaeppler, U.; Stiefl, N.; Schiller, M.; Vicik, R.; Breuning, A.; Schmitz, W.; Rupprecht, D.; Schmuck, C.; Baumann, K.; Ziebuhr, J.; Schirmeister, T. A new lead for nonpeptidic active-site-directed inhibitors of the severe acute respiratory syndrome coronavirus main protease discovered by a combination of screening and docking methods. *J. Med. Chem.* **2005**, *48*, 6832−6842.

(14) Ghosh, A. K.; Xi, K.; Ratia, K.; Santarsiero, B. D.; Fu, W.; Harcourt, B. H.; Rota, P. A.; Baker, S. C.; Johnson, M. E.; Mesecar, A. D. Design and synthesis of peptidemimetic severe acute respiratory syndrome chymotrypsin-like protease inhibitors. *J. Med. Chem.* **2005**, *48*, 6767−6771.

(15) Shie, J. J.; Fang, J. M.; Kuo, C. J.; Kuo, T. H.; Liang, P. H.; Huang, H. J.; Yang, W. W.; Lin, C. H.; Chen, J. L.; Wu, Y. T.; Wong, C. H. Discovery of potent anilide inhibitors against the severe acute respiratory syndrome 3CL protease. *J. Med. Chem.* **2005**, *48*, 4469−4473.

(16) Chen, L. R.; Wang, Y. C.; Lin, Y. W.; Chou, S. Y.; Chen, S. F.; Liu, L. T.; Wu, Y. T.; Kuo, C. J.; Chen, T. S. S.; Juang, S. H. Synthesis

and evaluation of isatin derivatives as effective SARS coronavirus 3CL protease inhibitors. *Bioorg. Med. Chem. Lett.* **2005**, *15*, 3058−3062.

(17) Shie, J. J.; Fang, J. M.; Kuo, T. H.; Kuo, C. J.; Liang, P. H.; Huang, H. J.; Wu, Y. T.; Jan, J. T.; Cheng, Y. S.; Wong, C. H. Inhibition of the severe acute respiratory syndrome 3CL protease by peptidomimetic $\alpha,\beta$-unsaturated esters. *Bioorg. Med. Chem.* **2005**, *13*, 5240−5252.

(18) Jain, R. P.; Petterson, H. I.; Zhang, J.; Aull, K. D.; Fortin, P. D.; Huitema, C.; Eltis, L. D.; Parrish, J. C.; James, M. N. G.; Wishart, D. S.; Vederas, J. C. Synthesis and evaluation of keto-glutamine analogues as potent inhibitors of severe acute respiratory syndrome $3CL^{pro}$. *J. Med. Chem.* **2004**, *47*, 6113−6116.

(19) Ghosh, A. K.; Xi, K.; Grum-Tokars, V.; Xu, X.; Ratia, K.; Fu, W.; Houser, K. V.; Baker, S. C.; Johnson, M. E.; Mesecar, A. D. Structure-based design, synthesis, and biological evaluation of peptidomimetic SARS-CoV $3CL^{pro}$ inhibitors. *Bioorg. Med. Chem. Lett.* **2007**, *17*, 5876−5880.

(20) Regnier, T.; Sarma, D.; Hidaka, K.; Bacha, U.; Freire, E.; Hayashi, Y.; Kiso, Y. New developments for the design, synthesis and biological evaluation of potent SARS-CoV $3CL^{pro}$ inhibitors. *Bioorg. Med. Chem. Lett.* **2009**, *19*, 2722−2727.

(21) Bacha, U.; Barrila, J.; Velazquez-Campoy, A.; Leavitt, S. A.; Freire, E. Identification of novel inhibitors of the SARS coronavirus main protease $3CL^{pro}$. *Biochemistry* **2004**, *43*, 4906−4912.

(22) Chou, C. Y.; Chang, H. C.; Hsu, W. C.; Lin, T. Z.; Lin, C. H.; Chang, G. G. Quaternary structure of the severe acute respiratory syndrome (SARS) coronavirus main protease. *Biochemistry* **2004**, *43*, 14958−14970.

(23) Lee, T. W.; Cherney, M. M.; Huitema, C.; Liu, J.; James, K. E.; Powers, J. C.; Eltis, L. D.; James, M. N. G. Crystal structures of the main peptidase from the SARS coronavirus inhibited by a substrate-like aza-peptide epoxide. *J. Mol. Biol.* **2005**, *353*, 1137−1151.

(24) Yang, S.; Chen, S. J.; Hsu, M. F.; Wu, J. D.; Tseng, C. T. K.; Liu, Y. F.; Chen, H. C.; Kuo, C. W.; Wu, C. S.; Chang, L. W.; Chen, W. C.; Liao, S. Y.; Chang, T. Y.; Hung, H. H.; Shr, H. L.; Liu, C. Y.; Huang, Y. A.; Chang, L. Y.; Hsu, J. C.; Peters, C. J.; Wang, A. H. J.; Hsu, M. C. Synthesis, crystal structure, structure-activity relationships, and antiviral activity of a potent SARS coronavirus 3CL protease inhibitor. *J. Med. Chem.* **2006**, *49*, 4971−4980.

(25) Lee, C. C.; Kuo, C. J.; Ko, T. P.; Hsu, M. F.; Tsui, Y. C.; Chang, S. C.; Yang, S.; Chen, S. J.; Chen, H. C.; Hsu, M. C.; Shih, S. R.; Liang, P. H.; Wang, A. H. J. Structural basis of inhibition specificities of 3C and 3C-like proteases by Zinc-coordinating and peptidemimetic compounds. *J. Biol. Chem.* **2009**, *284*, 7646−7655.

(26) Al-Gharabli, S.; AliShah, S. T.; Weik, S.; Schmidt, M. F.; Mesters, J. R.; Kuhn, D.; Klebe, G.; Hilgenfeld, R.; Rademann, J. An efficient method for the synthesis of peptide aldehyde libraries employed in the discovery of reversible SARS coronavirus main protease (SARS-CoV $M^{pro}$) inhibitors. *ChemBioChem* **2006**, *7*, 1048−1055.

(27) Akaji, K.; Konno, H.; Onozuka, M.; Makino, A.; Saito, H.; Nosaka, K. Evaluation of peptide-aldehyde inhibitors using R188I mutant of SARS 3CL protease as a proteolysis-resistant mutant. *Bioorg. Med. Chem.* **2008**, *16*, 9400−9408.

(28) Castro, B.; Dormoy, J. R.; Evin, G.; Selve, C. Reactifs de couplage peptidique- 1-hexafluorophosphate de benzotriaolyl *N*-oxytrisdimethylamino phosphonium (BOP). *Tetrahedron Lett.* **1975**, *16*, 1219−1222.

(29) Fehrentz, J. A.; Paris, M.; Heitz, A.; Velek, J.; Liu, C. F.; Winternitz, F.; Martinez, J. Improved solid phase synthesis of C-terminal peptide aldehydes. *Tetrahedron Lett.* **1995**, *36*, 7871−7874.

(30) Tanaka, M.; Oishi, S.; Ohno, H.; Fujii, N. A novel oxazolidine linker for the synthesis of peptide aldehydes. *Int. J. Pept. Res. Ther.* **2007**, *13*, 271−279.

(31) Vazquenz, J.; Albericio, F. A convenient semicarbazide resin for the solid-phase synthesis of peptide ketones and aldehydes. *Tetrahedron Lett.* **2006**, *47*, 1657−1661.

(32) (a) Yao, W.; Xu, H. Y. Solid-phase synthesis of peptide aldehydes directly on acetal resin. *Tetrahedron Lett.* **2001**, *42*, 2549−2552. (b) The effect of the linker length and further optimization of the reaction conditions are now underway.

(33) Rink, H. Solid-phase synthesis of protected peptide fragments using a trialkoxy diphenylmethylester resin. *Tetrahedron Lett.* **1987**, *28*, 3787−3790.

(34) Barrila, J.; Gabelli, S. B.; Bacha, U.; Amzel, L. M.; Freire, E. Mutaition of Asn28 disrupts the dimerization and enzymatic activity of SARS $3CL^{pro}$. *Biochemistry* **2010**, *49*, 4308−4317.

(35) The binding mode of most potent inhibitor **31** was presented in PDB code 3AVZ.